

Numerical investigation of marsh terracing design parameters to optimize performance as a coastal restoration technique

Katelyn A. Keller^{*}, Kelin Hu, Ehab A. Meselhe

Tulane University of Louisiana, Department of River-Coastal Science and Engineering, New Orleans, LA, 70118, USA

ARTICLE INFO

Keywords:

Marsh terracing
Delft3D
Vermilion bay
Coastal restoration
Natural and nature based features

ABSTRACT

Marsh terracing is a newly implemented coastal restoration technique utilized within the Northern Gulf of Mexico, particularly the Louisiana Coast. Its application is intended to combat the devastating land loss rates currently occurring as a result of sea level rise, land subsidence, and anthropogenic alterations to the system. The technique involves dredging in-situ subtidal marsh soils and placing the excavated material into subaerial berms, or terraces, adjacent to the borrow pit. There is significant research addressing the ecological benefits of marsh terracing, such as increased marsh edge, enhanced bio productivity, and improved habitability for nekton and waterbird species. However, there is a lack of research investigating the proposed hydrodynamic benefits of marsh terracing, decreased shoreline erosion and marsh emergence. This study aimed to (1) quantify the ability of marsh terracing to reduce shoreline erosion, (2) create emergent marsh and (3) provide a set of metrics to assess project performance and determine the optimal terrace configuration for a specific site. The study site, Four Mile Canal Terracing and Sediment Trapping in Vermilion Bay, Louisiana, was analyzed through the creation of a 2D numerical model using Delft 3D Flexible Mesh. Coupling of D-Flow and D-Waves allowed for the analysis of high-resolution flow and wave dynamics within terrace configurations. Following model creation and utilization, six hypothetical terrace configurations were examined using post-processing tools and developed metrics. Site specific conclusions were drawn for the terrace configurations within Vermilion Bay. However, the numerical modeling methods and performance metrics presented herein provide a methodology that can be used to determine the optimal configuration for any terrace project site and provide the most beneficial use of project funding.

1. Introduction

A combination of sea level rise, land subsidence, and anthropogenic alterations to coastal systems has created devastating land loss rates throughout the marsh wetlands of the Northern Gulf of Mexico. This challenge prompted unprecedented investments in restoration projects along the Louisiana coast, many without formal design protocol. Louisiana coastal wetland loss is among the highest on earth with an estimated loss of 1.2 million acres since 1932 and a projected loss of another 1.4 million acres by the year 2067 (Couvillion et al., 2017). Coastal restoration projects implemented to combat the loss of this fragile and valuable ecosystem include bank stabilization, oyster reef creation, sediment diversions, marsh creation, and shoreline protection (Coastal Protection and Restoration Authority of Louisiana, 2017). Furthermore, a recent shift towards more sustainable engineering has led to a newer category of restoration projects termed Natural and Nature-Based

Features (NNBF). These types of projects draw from the natural capacity of a coastal system to reduce flood impacts and land loss. Examples include oyster reefs, barrier island creations, beach renourishment, and vegetated marsh features. NNBF mimic the characteristics of a natural system but are engineered and constructed through human design (Temmerman et al., 2013; U.S. Army Corps of Engineers, 2015).

Marsh terracing is one of these new nature-based coastal restoration techniques, with the first Louisiana project execution documented by Underwood et al. (1991). In their study, a collection of existing marsh creation concepts, including baffle systems, breakwaters, and vegetative plantings, was combined into one feature to create the first terrace project. Baffle systems of ridges have been used in the Netherlands for hundreds of years to influence sedimentation. Breakwaters have been used around the world to reduce wave erosion of leeward shores. Furthermore, vegetative plantings have been long recognized as an approach to stabilize dunes, reduce wave energy, and increase

^{*} Corresponding author. 1408 Sylvia Avenue, Metairie, LA, 70005, USA.

E-mail address: kkeller8@tulane.edu (K.A. Keller).

sedimentation. The synergistic combination of these features in the form of a terrace was hypothesized to create results greater than the sum of their individual components (Underwood et al., 1991).

The technique of terracing involves dredging in-situ subtidal marsh soils and compacting the soil in subaerial berms adjacent to the borrow pit. After construction, the ridges are often planted with native marsh vegetation, such as *Spartina alterniflora*, to promote structural stability and encourage settling of suspended sediment in the water column. The segmented ridges are designed at neighboring marsh elevation to allow for periodic tidal inundation of the terrace and associated vegetation. Typically, they are designed following a nearby reference project and configured perpendicular to the predominant wind direction. There are a variety of configurations that can be created out of these ridges including chevron, grid, irregular, and linear configurations (Fig. 1).

There are two main goals of terracing: (i) when bordering a coastline, terraces may decrease wave fetch and prevent erosion on the leeward coast and (ii) when placed next to an adequate sediment source, slowed velocities may allow particles to settle and increase bed elevations through deposition. In some instances, a terracing arrangement could achieve both goals if designed and configured properly.

Despite nearly 30 years of implementation and over 100 terrace fields built across the Northern Gulf of Mexico (Ducks Unlimited, 2018), very few studies have been conducted to evaluate their hydrodynamic performance as a marsh reclamation tool. The studies that are available focus on assessing land area change using aerial imagery or their ability to ecologically enhance marsh environments (Brasher, 2015). Aerial imagery studies suggest that deposition is more predominant than erosion within 20 evaluated marsh terrace sites. The sites with the most

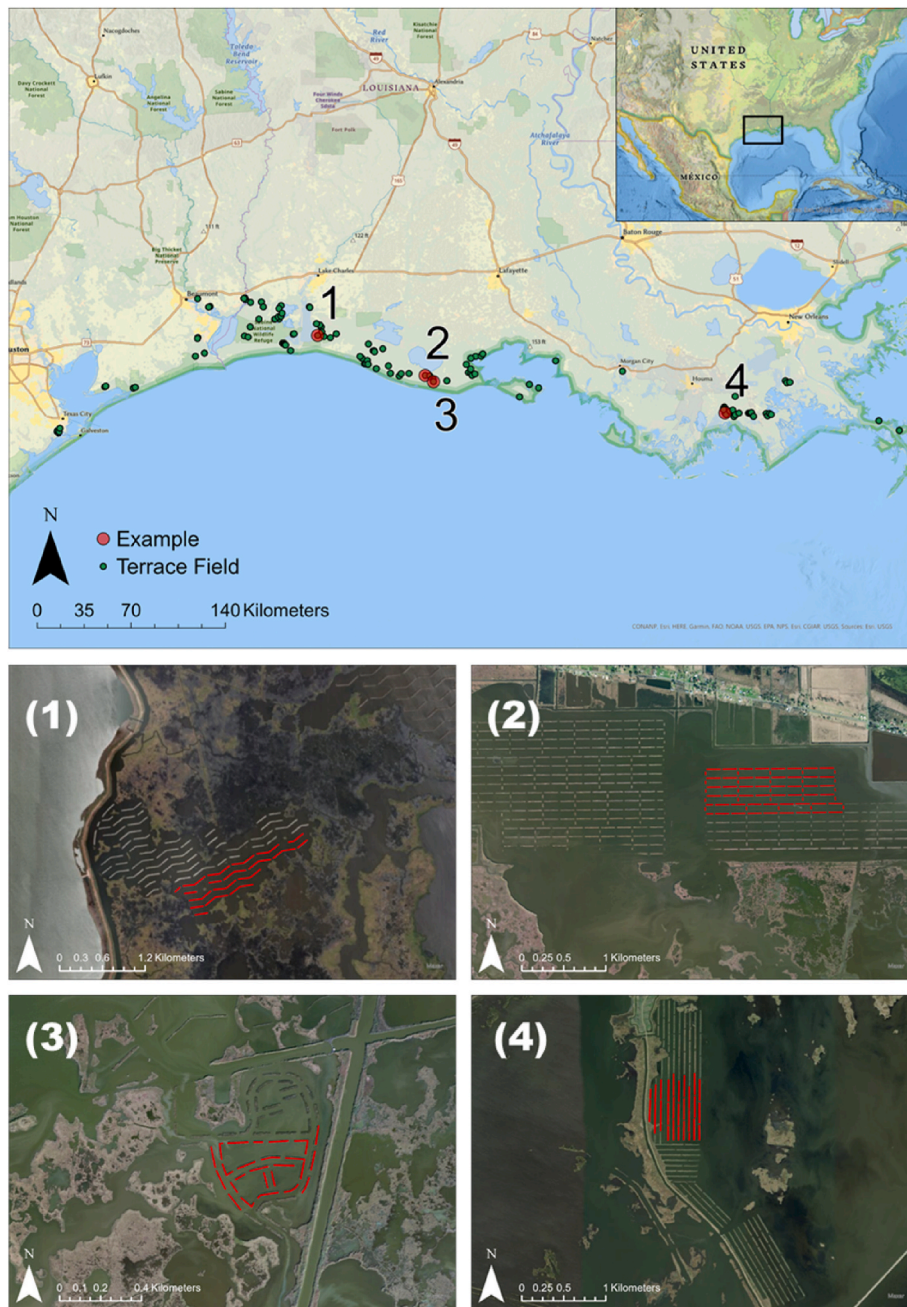


Fig. 1. Example Terrace Configurations. The top map shows the Ducks Unlimited, 2018 geodatabase for 116 terrace locations across the Louisiana coast and parts of the Texas coast. Four examples, with terrace crowns highlighted in red, were chosen and presented to demonstrate the diversity of terrace layouts. Outlined in red for ease of viewing are (1) chevron, (2) grid, (3) irregular, and (4) linear configurations.

deposition present are those which have high channel density and, subsequently, a high sediment supply (Osorio et al., 2020). O'Connell and Nyman (2010) evaluated a single site using aerial imagery for four years post-construction and found extensive mudflat development near project features, indicating the potential utility of terracing (O'Connell and Nyman, 2010; Brasher, 2015). These studies suggest that terracing can improve marsh habitat but give little insight into how different variables, including water depth, terrace elevation and width, and terrace configuration, affect the rate of land change.

The erosive nature of wind waves on shorelines is heavily attributed to fetch distances (Allison et al., 2017). Terracing has the capability to disrupt the wind pattern, reduce fetch and associated bed stresses, and break the negative feedback cycle of marsh collapse. Fig. 2 shows this idea of attenuating wave energy by reducing fetch distances. Multiple studies have used aerial imagery combined with wind and marsh soil sampling methods to determine that the most effective way to interrupt fetch is to orient terracing perpendicular to the most prevalent wind conditions (French, 2020; Matthews, 2020). Matthews (2020) also attempted to gauge sediment accretion through analyzing a synthetic hydrodynamic model for bed shear stress and velocity patterns within linear, grid, and chevron terrace configurations. The study suggests that an energy shadow zone decreases both velocity and bed shear stress within the area directly behind a terrace berm. The areas around the edge of terracing experience higher velocities and presumably erosion. However, the exact configuration that creates this condition differs by site location. French (2020) and Matthews (2020) both conclude that the best configuration for terracing along the Gulf Coast is chevron, as it effectively blocks winds in four possible directions.

While the studies involving marsh terrace performance and design remain limited, there is sufficient information addressing the ecological impact of implementation. There is consistent data that documents increased estuarine nekton use of terraced sites versus non-terraced sites. A study completed in the Sabine National Wildlife Refuge concluded 1.5–55x more biomass in terraced than reference sites, indicating increased habitat quality and fishery production (Rozas and Minello, 2001). Similarly, waterbird density increased in terraced sites by 75% when compared to reference sites (O'Connell and Nyman, 2010). Increased marsh edge by terracing can also provide more habitat for fish and waterbird species, supporting valuable fisheries and wildlife habitat across the Louisiana coast.

Despite the reports highlighting the potential benefits of terracing,

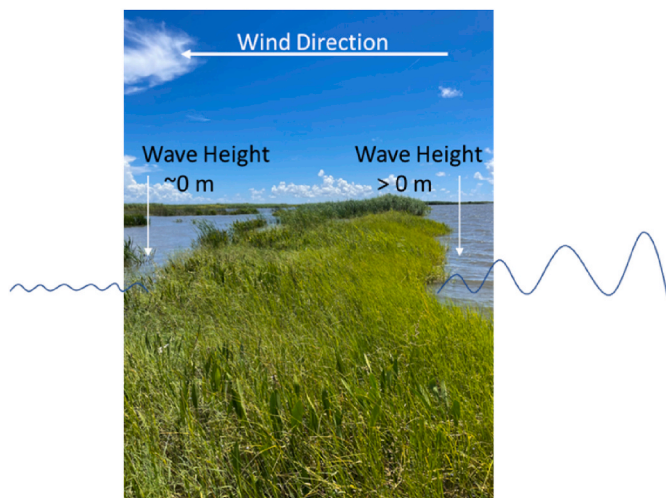


Fig. 2. Wave Attenuation by Terracing. This picture of a terrace berm was captured on a site visit to Vermilion Bay. On the right, waves approaching from offshore are successfully attenuated by the berm disrupting the wind fetch. On the left, wave heights are much smaller and must re-generate by beginning the wave propagation process over.

there are several projects that did not produce these expected outcomes. Miller and Guidry (2011) examined a terracing site that deteriorated and was deemed ineffective by the end of the first-year post-construction monitoring. In their final report, degradation was attributed to high water depth, excessive spacing between terracing, undersized typical sections, and a lack of time for berm consolidation and vegetation prior to heavy wave attack. Although classified as a failure, the lessons learned in this project and the inability to envision these issues pre-construction highlight the gap in knowledge about the design of these structures.

The paucity of information studying terrace project hydrodynamics has led to few design improvements, and in-depth analysis of structure design and performance is crucial for future design recommendations. If the construction of terracing is to be continued along the Louisiana coast, their benefits and costs must be quantified for stakeholders and decision makers. This study provides insight into the role of various terrace geometric properties on their ability to (i) attenuate wave height and decrease shoreline erosion and (ii) reduce water velocities and induce deposition. Ultimately, creating a set of metrics to maximize terrace performance and minimize project costs for future projects is a major goal of the present study. The aim of this study is to setup a high resolution hydrodynamic numerical model and perform a thorough analysis of marsh terracing projects along the Louisiana coast. The research questions to be addressed in this study are.

- What is the magnitude of wave energy attenuation by terracing compared to length of terrace constructed, measurable through the analysis of wave power reaching the leeward coast?
- What is the ratio of depositional area within terrace configurations compared to area of terrace constructed, measurable through the calculation of total area below a depositional bed shear stress threshold?
- How can terrace fields be designed in the future to optimize their ability to attenuate waves and create marsh, measurable by comparing the output values of questions A and B for various configurations and creating metrics to quantify project costs versus project benefits?

2. Numerical model

2.1. Model description

The numerical model Delft3D Flexible Mesh (2021.03) was used to couple a flow model and a wave model using high-resolution two-dimensional, depth-averaged grids (Deltares, 2019a,b). Delft3D is a hydrodynamic model that solves for water level, flow velocities, and a host of other derived variables, e.g., bed shear stress, resulting from imposed meteorological and tidal conditions. There are several integrated modules within Delft3D that simulate fluid flow, wave generation and propagation, sediment transport, morphological changes, and water quality.

For this project, a hindcast flow model was created using the D-Flow Module. The module's ability to handle unstructured grids with adequate computational speed and accuracy allowed for hydrodynamic computations within the complex terrace geometries. D-Flow solves the Navier-Stokes equations for mass and momentum conservation of an incompressible fluid, under the shallow water and Boussinesq assumptions. The base form of both the mass (1) and momentum (2) depth-averaged, shallow water equations was given by Herman et al. (2011) as:

$$\frac{\partial H}{\partial t} + \nabla \cdot (H \vec{u}) = q \quad (1)$$

$$\frac{\partial \vec{u}}{\partial t} + \text{adv}(\vec{u}) + g \nabla \zeta + c_f \vec{u} \|\vec{u}\| + 2\Omega \times \vec{u} = d \quad (2)$$

Where H is total water depth, ζ is the water level relative to a reference plane, \vec{u} is the depth-averaged horizontal velocity vector, ∇ is the horizontal gradient operator, Ω is the earth rotation vector, t is time, and $\text{adv}(\vec{u})$ is the advection term. The right-hand side q contains source terms and d contains external forcing. The constants g and c_f denote the gravity constant and bottom-friction coefficient, respectively (Herman et al., 2011). More information on the governing processes can be found in the D-Flow User Manual (Deltares, 2019a,b).

The D-Waves Module was chosen for its ability to simulate near-shore short wave modeling. D-Waves is based on the third generation SWAN, Simulating WAVes Nearshore, calculation core and is capable of computing wave propagation, wave generation by wind, dissipation, and nonlinear wave-wave interactions. SWAN solves the spectral action balance equation (Equation (3)) to calculate wave parameters given meteorological and hydrodynamic forcings.

$$\frac{\partial N}{\partial t} + \nabla_{\vec{x}} \cdot \left[\left(\vec{c}_g \vec{U} \right) N \right] + \frac{\partial \sigma N}{\partial \sigma} + \frac{\partial c_\theta N}{\partial \theta} = \frac{S_{\text{tot}}}{\sigma} \quad (3)$$

N is the wave action density at a single point in space, which is conserved during wave propagation. \vec{U} is the ambient current, \vec{c}_g is the group velocity, t is time, ∇ is the horizontal gradient operator, the variable c_σ and c_θ are the propagation velocities in spectral space (σ, θ), where σ is angular frequency and θ is direction. S_{tot} is the of source terms which generate, dissipate, or redistribute wave energy at a point (SWAN, 2021). More background on governing equations can be found in the D-Waves User Manual (Deltares, 2019a,b).

Through an online coupling of the two suites, the effect of wave conditions on flow hydrodynamics (via water level changes, enhanced turbulence, and enhanced bed shear stress) and flow on waves (via water level changes and current refraction) is updated at a set 60-min communication interval, although this interval can be refined for more frequent information exchange. Additional Deltares tools used in the study include RGFRID for grid generation, QUICKIN for data interpolation to the computational grid, and QUICKPLOT for post-processing and output visualization.

2.2. Model domain

Vermilion Bay, Louisiana was chosen as the study site for this

analysis due to the estuary’s established historical pattern of marsh edge erosion, proximity to an adequate sediment source (namely the Tech-Vermilion and Atchafalaya Rivers), and diverse use of terrace designs and objectives in extant projects. The estuary was historically nourished by the Vermilion River, but navigational dredging in the mid-1900’s and subsequent spoil bank creation cut off the adjacent marsh from its sediment sources. The main cause of shoreline erosion within the estuary was wind and wake energy, leading to an estimated pre-terracing marsh edge erosion rate of 2.4 m/year (8 ft/year) (Louisiana Coastal Wetlands Conservation and Restoration Task Force, 2017).

The implemented terrace project that is the focus of the present study is titled Four Mile Canal Terracing and Sediment Trapping (TV-18) and includes approximately 4 047 m² (2000 acres) within Little White Lake (LWL) and the western part of Little Vermilion Bay (LVB) just west of Four Mile Canal (Fig. 3). The terrace configuration includes two sets of terraces, each designed with different restoration goals. The linear design within Little White Lake consists of 12,283 linear meters (40,300 ft) of terrace and contours the shoreline with the intent to shorten wave fetch and attenuate wave energy at the leeward coast. The design within Little Vermilion Bay includes 8580 linear meters (28,150 ft) in total length and follows a fishnet configuration, designed to act as a baffle for sediment-laden flow entering from the Vermilion River. This project was completed in May 2004 through the Coastal Wetlands Planning, Protection and Restoration Act (CWPPRA) program for a total funding cost of \$2.33 million (Thibodeaux et al., 2004). This leads to an estimated cost of \$112 per linear meter of terrace created, a relatively low cost for a marsh restoration project.

2.3. Model setup

Using Delft3D Flexible Mesh Flow and Wave Suites, the characteristics of the area post-project were replicated, and the setup is shown in Fig. 4. The primary area of interest is the terracing within Little White Lake and Little Vermilion Bay, but the domain extents are significantly larger to prevent any changes within the model from propagating back to the boundaries. The flow model domain (Fig. 4a) extends from the mouth of the Vermilion River to Cypremort Point and Southwest Pass, encompassing Weeks Bay, Vermilion Bay, Little White Lake, and Little Vermilion Bay. The flow grid contains 555,318 cells ranging in resolution from 2.5 m to 364 m, with the most refinement within the terrace

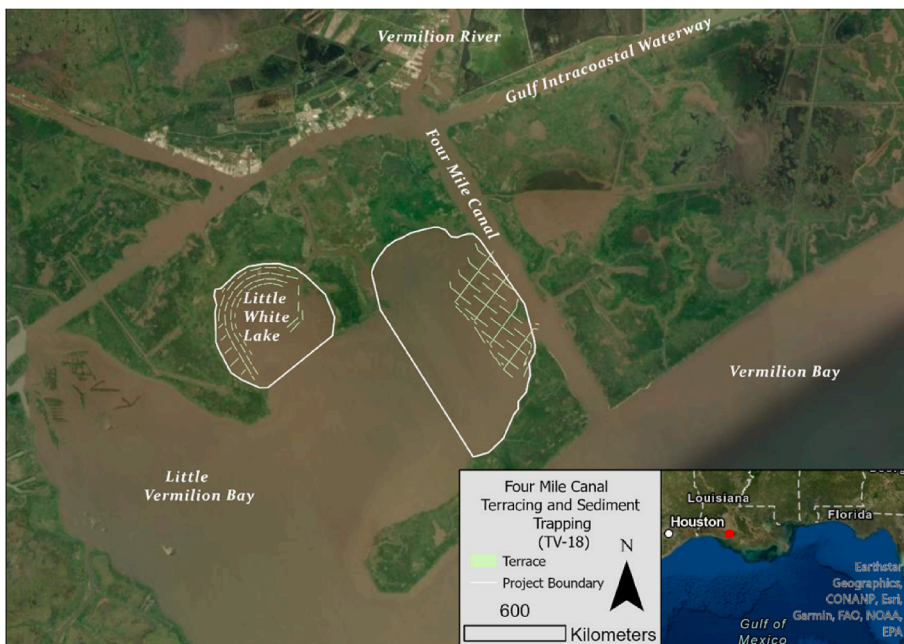


Fig. 3. Four Mile Canal Terracing and Sediment Trapping Conceptual Project Design. Fig. 3 shows the conceptual layouts of both sets of project terracing reproduced following the CWPPRA TV-18 Fact Sheet (Louisiana Coastal Wetlands Conservation and Restoration Task Force, 2017). The terrace outlines shown in green delineate the contoured linear terracing within Little White Lake and the fishnet terracing within Little Vermilion Bay. The white outlines the specified project boundaries. The inset map shows the location of this project (red dot) in relation to the Gulf Coast.

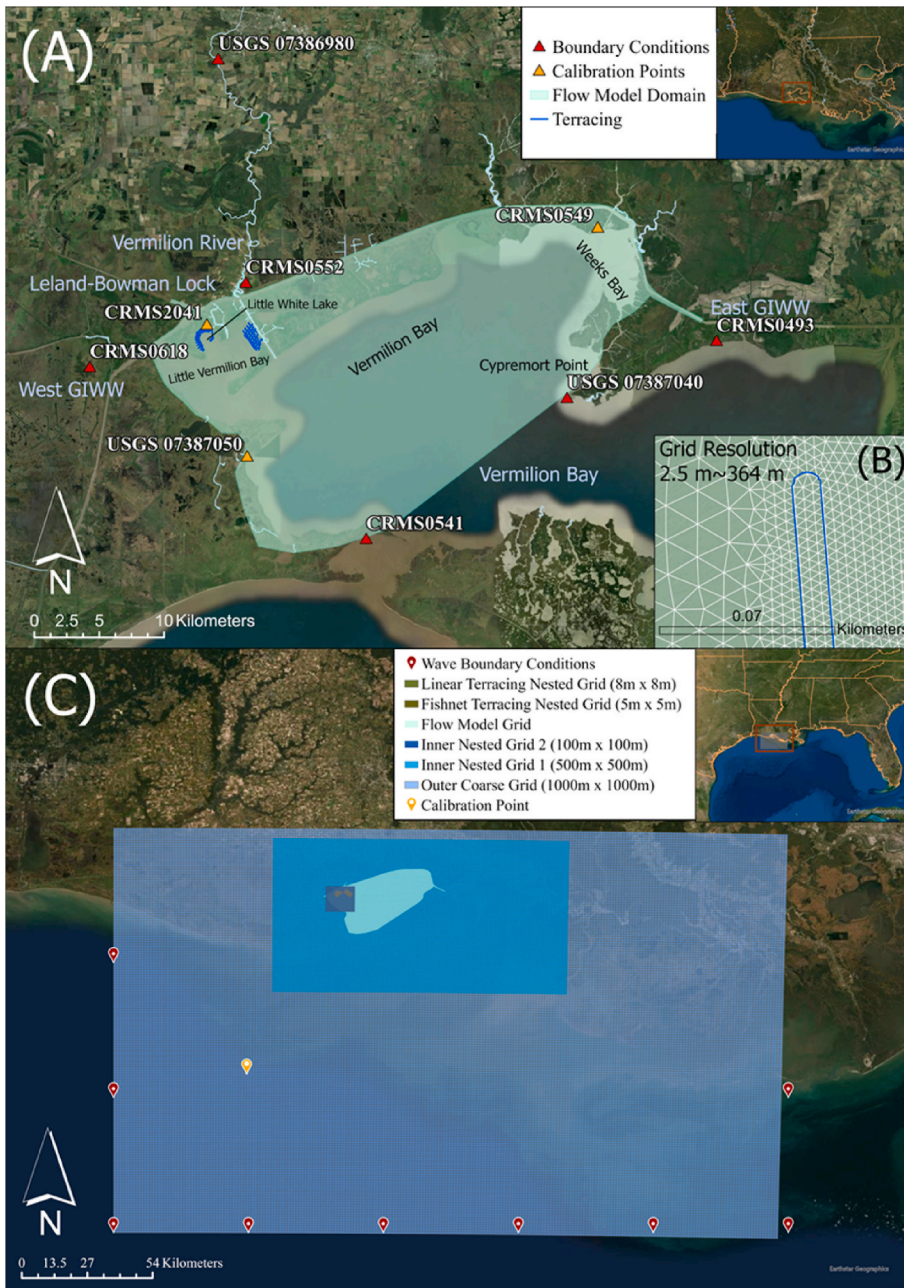


Fig. 4. Coupled Flow and Wave Model Setup. The flow model (A) extends from the mouth of the Vermilion River to Southwest Pass and Cypremort Point. There are five open boundaries and 3 calibration points marked in orange. (B) Shows the finest refinement of the grid on a terrace crown. The wave model (C) extends 100 km into the open Gulf of Mexico and includes five nested grids, refining towards the terrace areas of interest, with the locations of wave boundary forcings marked in red and the calibration point in orange.

areas of interest (Fig. 4b) and coarser cells elsewhere to save computational time. The wave model (Fig. 4c) extends nearly 100 km into the open Gulf to accurately simulate deep water waves reaching the estuary from the Northern Gulf of Mexico. The wave model uses a nested grid approach with five grids, coarsening from 5 m within the areas of interest to 1000 m in the open Gulf.

Model bathymetry was drawn from three sources to accurately replicate conditions within the open Gulf and within the refined terrace portions: 3×3 m USGS Coastal National Elevation Database (U.S. Geological Survey Coastal National Elevation Dataset, 2014), Gulf Intracoastal Waterway (GIWW) and Four Mile Canal U.S. Army Corps of Engineers navigational surveys (U.S. Army Corps of Engineers, 2014), and TV-18 project surveys and design plans (Aucoin and Associates, 2004). Wind data within the model is spatially uniform over all grids using data extracted from USGS station 07,387,040. To simulate bottom friction within the estuary, a Chezy's roughness coefficient of $75 \text{ m}^{0.5} \text{ s}^{-1}$ was assigned to open water and $65 \text{ m}^{0.5} \text{ s}^{-1}$ to marsh land, based on

previous modeling studies (Meselhe et al., 2022).

There are a total of five open boundaries within the flow model, four water level forcings and one discharge forcing, and three calibration points. Forcing conditions for the flow model were downloaded from the Coastal Information Management System (CIMS) database, which provided hourly hydrographic data, and through the National Water Information System (NWIS), which provided hourly water data for the flow calibration period (Coastal Protection and Restoration Authority of Louisiana, 2022; U.S. Geological Survey, 2001). The wave model has an open gulf boundary at the edges of the coarsest grid to be forced with ERA5 Reanalysis wave parameter data including significant wave height, wave period, and wave direction. ERA5 provided hourly estimates of wave parameters on a $0.5^\circ \times 0.5^\circ$ grid based on model data and global observations for the wave calibration period (Hersbach et al., 2018). The SWAN model applies the imposed offshore boundary wave parameters to a JONSWAP spectrum with a $\cos^2(\theta)$ directional distribution centered around the local wind direction. The water depths at the

location of this boundary were near 50 m. Time series graphs for the imposed boundary conditions can be found in Appendix A. All features are spatially referenced using UTM Zone 15 N and the vertical datum NAVD88. Table 1 summarizes the boundary conditions and corresponding datasets, which can be spatially referenced in Fig. 4.

2.4. Model calibration

After the hydrodynamic model was built, flow calibration efforts were focused on matching tidal water level fluctuations and salinity levels at the three calibration points: stations at CRMS 0549, CRMS 2041, and USGS 07387050 (Fig. 4). This was completed by appropriately choosing the Chezy roughness coefficient, which directly affects velocities and turbulence, throughout the model to achieve an acceptable margin of error between predicted and observed stages. Two categories of land type were chosen, marshland and open water, by assigning all depth values greater than 0 m to marshland and all values less than 0 m to open water. A value of $65 \text{ m}^{0.5} \text{ s}^{-1}$ was selected to represent marshland, and a value of $75 \text{ m}^{0.5} \text{ s}^{-1}$ was used to represent friction within open waters (Meselhe et al., 2022). These values are spatially portrayed in Fig. 5.

Salinity (as a conservative constituent) was analyzed during calibration efforts to ensure velocities within the model were captured reasonably. There was no velocity gage data within the model domain, so salinity movement acted as a proxy for examining the model's ability to mimic the flow dynamics. However, salinity was not activated during model runs as it is not significant for wave power or bed shear calculations, and excluding it increases computational efficiency. Note that salinity measurements are low for all calibration points (~1–3 ppt) as this is a freshwater estuary, while the salinity at the boundary was ~5–15 ppt. Thus, the exact high-frequency fluctuations are hard to capture, but it is important to observe if the model is able to produce the gradient from the saline boundary to the fresher interior. The flow calibration period ranged from June 1, 2019 to June 30, 2019 for diverse salinity and riverine discharge ranges and data availability purposes.

The wave model was also calibrated to ensure accurate simulations of wave energy. There was one offshore calibration point within the wave model at Trinity Shoal, La (Fig. 4). Both wave height and wave period were assessed at this point, specifically during events that may cause localized wave energy within the estuary. The default settings and parameters were adopted in the wave model. No specific adjustments were made to the calibration parameters within the wave model. The wave calibration period ranged from October 1, 2021 to November 1, 2021. The localized event chosen for calibration occurred October 26, 2021 00:00:00 to November 01, 2021 00:00:00 because it represented a localized wind event without surge, represented by lower wave periods and high wave heights.

Model performance metrics, including Root Mean Square Error

Table 1

Boundary Condition Data. Data station information for collected data used within the flow and wave models.

Site Name	Boundary Location	Data Type
Flow Model		
USGS 07387040	Vermilion Bay	Water Level
CRMS 0541	Vermilion Bay	Salinity
CRMS 0618	West GIWW	Water Level, Salinity
USACE Lock Data	Leland-Bowman Lock	Water Level
Wave Model		
USGS 07386980	Vermilion River	Discharge
CRMS 0552	Vermilion River	Salinity
CRMS 0493	East GIWW	Water Level, Salinity
USGS 07387040	Entire Domain	Wind Magnitude and Direction
ERA5 Reanalysis Data		
USGS 07387040	Entire Domain	Wave Height, Period, and Directional Spread
USGS 07387040	Entire Domain	Wind Magnitude and Direction

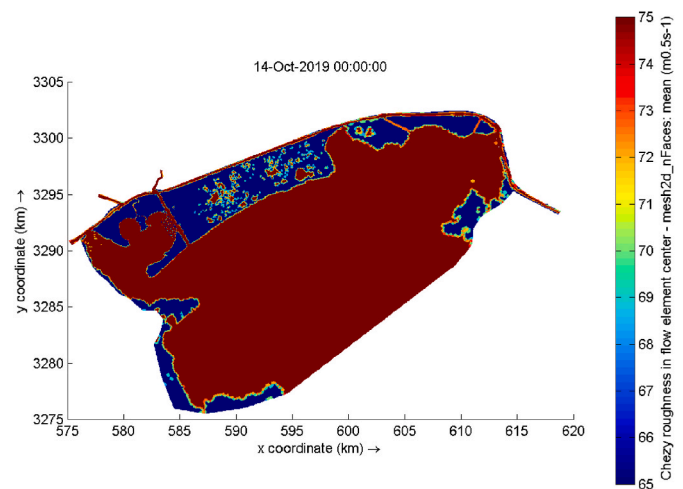


Fig. 5. Spatially Varying Bed Roughness Map. This figure shows the differences in the Chezy roughness coefficient throughout the flow model domain. Open water is visualized in red with a Chezy roughness coefficient of $75 \text{ m}^{0.5} \text{ s}^{-1}$ and marsh is visualized in blue with a Chezy roughness coefficient of $65 \text{ m}^{0.5} \text{ s}^{-1}$.

(RMSE), Bias, and the Pearson Product-Moment Correlation Coefficient, were calculated to determine the limits of model performance relative to calibration data. These statistics provide confidence in the model as a tool to predict the outcomes of simulations. Stage and wave height measurements were chosen for statistical analysis. The model outputs and observed values from the calibration period were used as the variables in the following metrics to evaluate the fitness between predicted and observed values. RMSE is a measure of the variation between predicted model data and observed values. The equation for RMSE is:

$$RMSE (\%) = \sqrt{\frac{\sum_{i=1}^n (P_i - O_i)^2}{n}} \quad (4)$$

P represents predicted values, O represents observed values, and n is the number of observations. A smaller RMSE percentage correlates to a better fit model. Here, the stage statistical values for the hydrodynamic model range from 0.06 to 0.09 m. The wave height statistical analysis resulted in a RMSE of 0.35 m. Bias determines whether the model consistently under or overestimates values, where a negative value represents underestimation and a positive value represents overestimation. The equation for bias is given by:

$$Bias = \frac{\bar{P} - \bar{O}}{\bar{O}} \quad (5)$$

\bar{P} is the mean of predicted values and \bar{O} is the mean of observed values. Here, the bias is close to 0 for all calibration points, indicating that this model does not over or underestimate stage values. Finally, the correlation coefficient measures the phasing difference between observed and predicted values, where a value of 1 is preferred. The correlation coefficient is given by:

$$r = \frac{\sum_{i=1}^n (\bar{P}_i - \bar{P})(\bar{O}_i - \bar{O})}{\sqrt{\sum_{i=1}^n (\bar{P}_i - \bar{P})^2} \sqrt{\sum_{i=1}^n (\bar{O}_i - \bar{O})^2}} \quad (6)$$

All calibration performance metrics fall within acceptable ranges, implying that the model is equipped to produce reasonable results in the chosen numerical experiments. Fig. 6 shows the stage and salinity time series for model predictions compared to observed values over the entire flow calibration month of June 2019 and the comparison of wave height and wave period time series over the localized wave event. Table 2 below shows the calculated stage performance metrics compared to ideal values (Meselhe and Rodrigue, 2013) (see Fig. 6) (see Table 2).

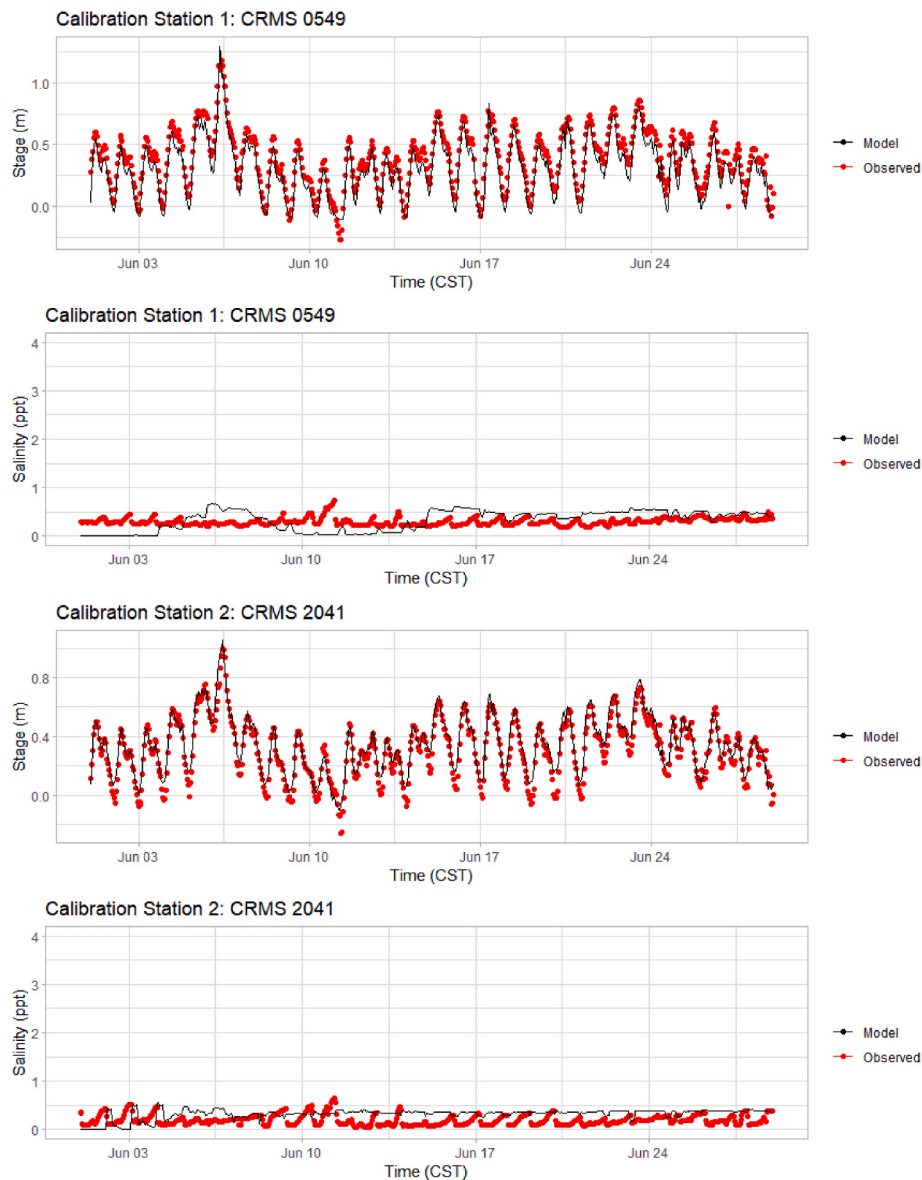


Fig. 6. Time Series for Flow and Wave Model Calibration. The calibration period for the wave model ranged from October 26, 2021 to November 1, 2021 and included both wave height and wave period. The calibration period for the flow model included the entire month of June 2019. The red points represent the observed (measured) values while the black line represents the modeled values.

3. Numerical experiments

3.1. Model Configurations

Model configurations were set up to assess the impact of terrace configuration on wave attenuation and sediment deposition. This was completed by altering the model bathymetry to replicate various hypothetical terrace configurations. Geometric properties including the terrace crown, berm, and borrow pit were created following design plans from neighboring terrace projects. To account for vegetation induced roughness changes along terrace crowns, the Chezy roughness coefficient was altered to match the various configurations. Each numerical experiment was run for a two-week simulation period ranging from October 1, 2019 00:00:00 to October 14, 2019 00:00:00, which imposed identical wave, water level, and wind conditions on each configuration.

Configuration 1 serves as the base simulation for following runs. It includes no terracing within Little White Lake, which allows for analysis of wave power reduction with and without terracing. It also includes the

as-built fishnet terrace configurations within Little Vermilion Bay, which was based off the TV-18 As-Built surveys (Aucoin and Associates, 2004) that defined the entire base of the terracing as 20 m (65.6 ft) in width and the crown as 6 m (19.6 ft) wide at an average of 1 m (3.3 ft) above NAVD88 in height. The borrow pit was artificially dredged to 3 m (9.8 ft) and placed on the leeward side of terracing. The remaining set of configurations followed the same terrace geometry but were constructed in different configurations.

Configuration 2 included a single linear row of terracing in Little White Lake based on the previously described TV-18 surveys and an increased width of the crown, base, and borrow pit within the fishnet terracing by 100% (doubled).

Configuration 3 included two linear rows of terracing in Little White Lake and a delta-splay terrace configuration within Little Vermilion Bay. The delta-splay configuration was based off a neighboring project, TV-12 Little Vermilion Bay Sediment Trapping, which included similar features mimicking a natural deltaic formation (Castellanos, 2003).

Configuration 4 included all the as-built terraces within Little White

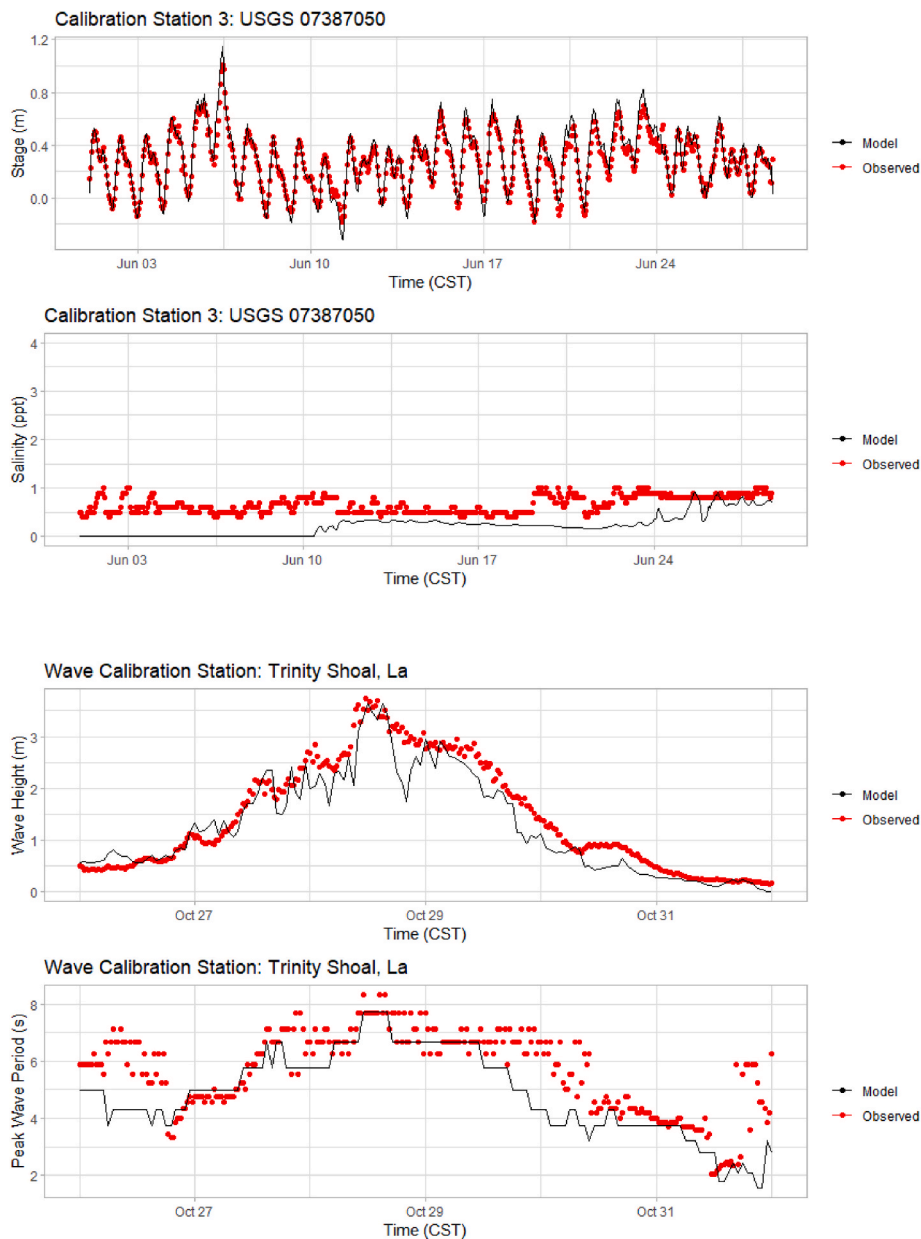


Fig. 6. (continued).

Table 2

Stage Performance Metrics. Performance metrics for statistical analyses included RMSE, Bias, and the Correlation Coefficient. All fell within acceptable ranges.

Stage and Wave Height Performance Metrics			
Station	RMSE (m)	Bias (%)	Correlation Coefficient
Observation Point 1: CRMS 0549	0.09	-20	0.98
Observation Point 2: CRMS 2041	0.06	11	0.97
Observation Point 3: USGS 07387050	0.06	8	0.97
Wave Height: Trinity Shoal, La	0.35	-12	0.96
Ideal Values	0	0	1

Lake, which consisted of four linear rows of terracing and five individual berms near the lake center following the flow path of the adjacent stream. Within Little Vermilion Bay, Configuration 4 included a grid configuration with gaps between berms to allow water and sediment

trapping based off the terracing in Pecan Island, Louisiana (Guidry and Thibodeaux, 2004).

Configuration 5 included circular terracing within Little White Lake and Little Vermilion Bay. This idea was based off the natural tree islands of the Florida Everglades, which effectively hold peat soils and marsh trees in a circular-like “ridge and slough” pattern (Ross et al., 2006). This type of restoration is also used in West Galveston Bay, namely Jumbile Cove, Starvation Cove, Dalehite Cove, Carancahua Cove, and Bird Island Cove, although the raised circular features are termed “marsh mounds” (Turner and Streever, 2002; O’Brien, 2003). Without appropriate post-project monitoring, success of this configuration is unknown, although continued implementation suggests some benefits.

Configuration 6 included a chevron configuration within both Little White Lake and Little Vermilion Bay, which was based off the terracing project in East Sabine Lake and has previously been hypothesized to be an optimal configuration for reducing wave energy (Balkum et al., 2003). Table 3 and Fig. 7 describe the configuration for each simulation.

Table 3
Description of Model Configurations. Each model simulation included a specific terrace configuration described below.

Simulation	Description of Configuration
Configuration 1	No terracing within LWL and as-built terracing (Fishnet) within LVB
Configuration 2	First row of linear terracing within LWL and 100% increased terrace width within LVB
Configuration 3	First and second row of linear terracing within LWL and delta-splay configuration within LVB
Configuration 4	As-built terracing (4 rows) within LWL and grid configuration within LVB
Configuration 5	Circular configuration within LWL and circular configuration within LVB
Configuration 6	Chevron configuration within LWL and chevron configuration within LVB

3.2. Analysis of wave power along shoreline

For each hypothetical simulation, the wave power reaching the shoreline along Little White Lake was calculated at 12 observation points dispersed along the coast. Wave power was calculated using linear wave theory (Sorenson, 2006). This method has been proven accurate in similar studies utilizing D-Wave outputs to solve for wave power near a shoreline (Parker, 2014). Wave power (P) can be calculated using Equation (7), which is a function of wave energy (E) and group wave celerity (C_g). Equation (8) solves for wave energy and is a function of water density (ρ), acceleration due to gravity (g) and significant wave height (H_s). Group celerity is defined in equation (9),

which is a function of wave classification number (n, equation (10)) and individual wave celerity (C, equation (11)). The following equations were used to obtain wave power at each time step, resulting in a time series of wave power at each observation point:

$$P = EC_g \tag{7}$$

$$E = \frac{1}{8} \rho g H_s^2 \tag{8}$$

$$C_g = nC \tag{9}$$

$$n = \frac{1}{2} \left[1 + \frac{\frac{4\pi d}{L}}{\sinh\left(\frac{4\pi d}{L}\right)} \right] \tag{10}$$

$$C = \frac{L}{T} \tag{11}$$

After each wave power time series was calculated, a comparison of wave power reduction for a specific wind event was analyzed. The localized wind event examined in this analysis ranged from October 9, 2019 12:00:00 to October 11, 2019 12:00:00. The event had wind directions ranging from 0° to 360° true north and magnitudes from 1.25 m/s to 12.9 m/s, a time series of which can be found in Appendix A. The coverage of wind directions present in this analysis period allows for a terrace performance prediction under any local wind event including northerly wind cold fronts and winds blowing from the south during tropical storms. The predominant wind directions (100°–200°) within



Fig. 7. Model Configurations. The figure conceptualizes the shapes of the terrace configurations for each of the six model simulations.

this period allowed for the greatest fetch and, therefore, the greatest wave energy experienced at the shoreline. The average wave power during the event for each configuration was compared to the average wave power during the event for the base configuration (Configuration 1, no terracing), giving a percent reduction of wave power due to terracing.

$$\text{Percent Reduction} : \frac{\overline{P_1} - \overline{P_x}}{\overline{P_1}} \times 100 \quad (12)$$

where P_1 is the wave power resulting from configuration one and P_x is the wave power from the remaining configurations 2 through 6. In this way, the ability of each configuration to attenuate wave energy can be assessed. In order to correlate wave power reduction values to the amount of land and funds necessary to build the terracing, the average wave power reduction in watts/m was compared to the linear length of terracing for that configuration.

To further relate wave power expended at the shoreline to project benefits, and therefore stakeholder involvement, the average wave power was related to shoreline erosion rates. Previous studies completed throughout the Louisiana coast have established a linear relationship between wave energy and marsh retreat rates. Specifically, these studies apply numerical models, satellite imagery, and field surveys to establish an empirical relationship between historical erosion rates and wave power in marshes with depths, wave conditions, and soil characteristics similar to the present study site. Here, two of those studies and their resulting empirical formulas (Equations (13) and (14)) were used to estimate the average shoreline erosion, y (m/year), for each configuration within Little White Lake (Allison et al., 2017; Trosclair, 2013). Equation (13) has three subsets each representing a different bulk density range, low (a), medium (b), and high (c), for marsh soils. This will result in a range of estimated erosion rates. The temporal averages resulting from the chosen two-day wind event calculated at observation points 2–9 were averaged spatially, resulting in one wave power value (watts) for each configuration. Those values were then used as the variable x in the equations below.

$$y = 0.05x + 2.03 \quad (13a)$$

$$y = 0.03x + 2.49 \quad (13b)$$

$$y = 0.05x + 2.18 \quad (13c)$$

$$y = 0.0351x + 0.0343 \quad (14)$$

It is important to note that the estimated shoreline erosion rates calculated through this analysis represent storm induced erosion rates. The equations here are used to extrapolate the erosion rates occurring during a localized wind event. This means that their values will be significantly higher than if calculated using the average wave power the shoreline experiences over a year. This analysis could also be applied to wave power values resulting from a year-long model simulation; however, it should be noted that such approach may not fully capture erosion induced by significant wind events.

3.3. Analysis of maximum bed shear stress

For each model configuration, a map was created of the maximum bed shear stress that occurred at each cell over the two-week simulation period. By setting a threshold for which erosion of estuarine silt particles are likely to occur, these maximum bed shear stresses can serve as a proxy for estimating potential depositional and erosional area within a terrace configuration. If a cell remained below the set threshold for the entire period of the simulation, the cell was classified as depositional. If a cell ever reached a bed shear stress above the threshold, it was classified as erosional. By calculating the area of each cell and the number of cells within each category, the total depositional versus erosional area

was then given. The bed shear stress thresholds for deposition were determined based on previous modeling efforts and in-situ measurements of bed shear stresses in a nearby marsh. In-situ marsh bed shear stresses were calculated in a previous study as a function of the bulk density values of collected samples, which found the average critical shear stress to be 0.2 Pa (French, 2020). Calibrating efforts for the morphodynamic component of a nearby estuary defined critical shear stresses as 0.15 Pa for silt (Baustian et al., 2018). Estuarine particles are cohesive in nature and prone to coagulation, which will tend to increase their threshold of erosion. Based on this, the critical bed shear stress for erosion of a silt particle was determined to be within the bounds of 0.15 Pa and 0.25 Pa, and thresholds of 0.15, 0.20, and 0.25 were analyzed in this study.

The ability of a terrace to produce depositional area and the cost of the project is inherently related to the amount of terrace area built. For this reason, the analysis of depositional area produced by each configuration considers the area of terracing required to build the berms. The terracing area was calculated by multiplying the width (W) of terrace by the length (L) of the configuration. The total depositional area created was then divided by the area of terracing to produce a dimensionless depositional area ratio (DAR) to be used for comparing configurations. A higher ratio will represent more depositional area created and less constructed terrace area required. Specifically, a larger DAR indicates a more efficient and economically feasible design.

$$\text{Depositional Area Ratio (DAR)} = \frac{\text{Depositional Area}}{\text{Terrace Area}} \quad (15)$$

It should be noted that since the model bathymetry is not changing with time, the results of this analysis will only reflect the performance of the as-built design and does not consider the performance after terrace erosion, consolidation, or movement has occurred.

4. Results

4.1. Wave power results

For the two-week simulation period occurring October 1, 2019 through October 14, 2019, the wave power ranged from 0 W/m to nearly 150 W/m. The higher wave powers correlate to localized wind events within the system. As aforementioned, the localized wind event examined in this analysis ranged from October 9, 2019 12:00:00 to October 11, 2019 12:00:00 and included wind directions ranging from 0° to 360° and magnitudes from 1.25 m/s to 12.9 m/s. Fig. 8 below shows a time series of wave power (watts/m) over the event for selected observation points 1, 3, 5, 7, and 10 with the percent reduction by each configuration given. Wave power time series for all 12 observation points can be found in Appendix B. Configuration 1 (no terracing present) serves as the base to which all following configurations are analyzed for percent reduction.

Observation points 1–9 show relatively higher wave powers than observation points 10–12 due to the shape of the embayment and related fetch distances. Wave propagation within this estuary occurs over a longer distance when coming from angles around 100°–200° true north. Observation point 1 shows no reduction for any configuration as it lies out of the terrace protection. Observation point 3 shows the most reduction at 85% from the first line of terracing (Configuration 2), with subsequent reductions being much smaller. However, Configurations 3–6 show almost full reduction of wave energy. Observation point 5, which is placed between a terrace gap, exhibits the most reduction after two linear rows are added (Configuration 3), although a 64% reduction is present from the first linear row (Configuration 2). Observation point 7 which lies directly behind a terrace berm in the first linear row receives almost full reduction (97%), by adding only one row of terracing. It is important to note that these reductions represent the efficacy immediately after building, and reductions will begin to decrease as wave power erodes the terrace.

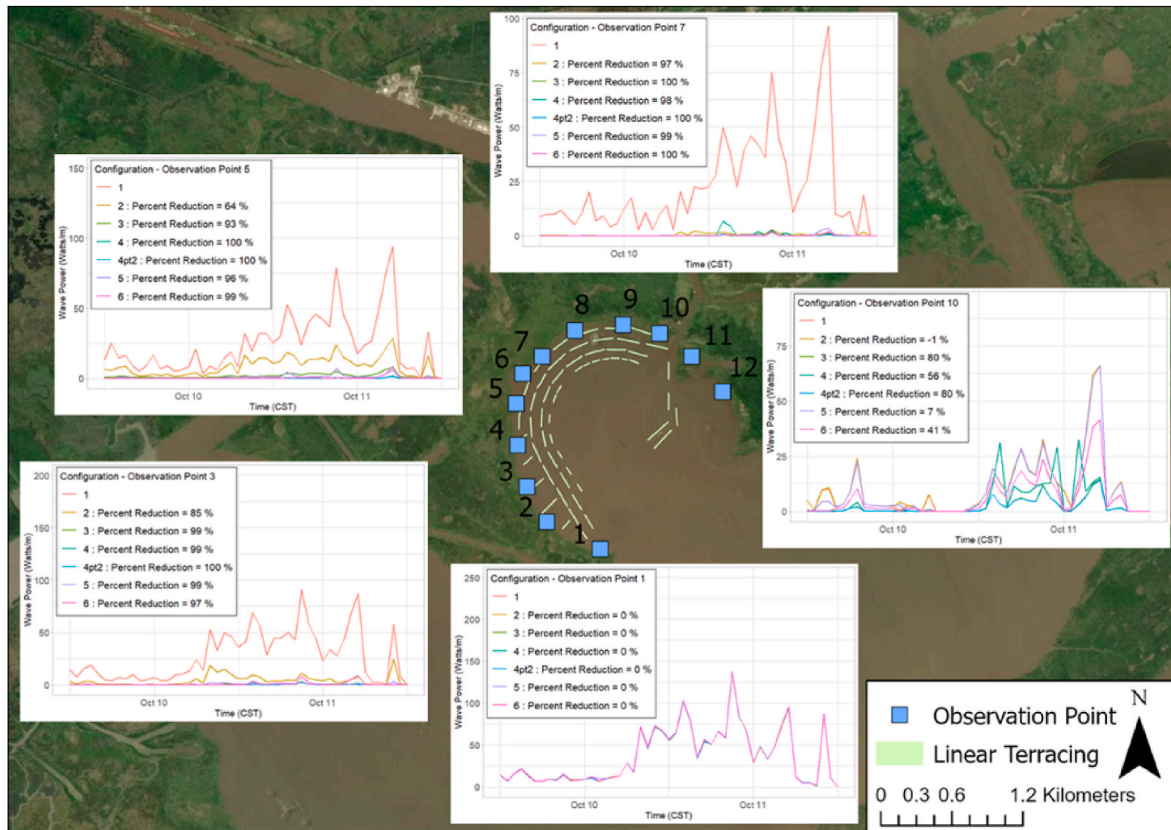


Fig. 8. Wave Power Reduction Analysis. The figure shows the time series, colored by model configuration, at observation points 1, 3, 5, 7, and 10. The locations of the observation points are represented by the blue squares on the map center. Note that this map displays the configuration of the full linear terracing (Configuration 4) for reference, but the configuration is changing with each run. The percent reduction by each configuration is shown in the left corner of each graph.

Observation point 10, which is placed at the eastern end of terracing layout, reveals an interesting pattern. The wave power present at the shoreline from the full set of terracing (Configuration 4) is higher than the wave power produced by only two linear rows (Configuration 3). The percent reduction decreases from 80% to 56%. Further analysis shows that the placement of the terracing at the center of LWL, following the flow path of the adjacent stream, tended to direct wave energy around and behind the eastern side of the configuration. This led to a channelization of wave energy at observation point 10. This can be understood by looking at the reduction of Configuration 4 pt. 2, which represents the wave power resulting from a simulation with only linear terracing and removal of the individual berms in the middle of LWL. The wave power reduction increases back to 80% after removal of the extra berms.

Although wave power is not the only variable responsible for marsh edge erosion, it is a known significant driver of wetland loss in Louisiana (Allison et al., 2017). Multiple previous studies have related retreat rates to wave energy expended at the shoreline, and empirical formulas have been developed from resulting trends (Trosclair, 2013; Allison et al., 2017). Table 4 below presents two of those empirical formulas, with the wave powers from this study as the driver for erosion. Here, wave power was averaged across Configurations 2–9, resulting in a temporally and spatially averaged wave power within Little White Lake (see Table 4).

The associated erosion rates range from 3.2 m/year for the configuration without any terracing to nearly 0 m/year as more berms are added to the configuration. The rather high erosion rates are representative of the storm induced erosion. These significant rates serve to examine the shoreline retreat occurring during a storm event, and do not represent a yearly average.

A comparison of terrace length and wave power reduction in watts/m reveals a similar trend throughout observation points. As the length

Table 4

Average Wave Power and Associated Shoreline Erosion Rates. The average wave power used to calculate erosion rates is a temporal and spatial average for each configuration. Two previous empirical formulas relating erosion and wave power were used.

Configuration	Average Wave Power (Watts/m)	Associated Erosion (m/year) (Allison et al., 2017)	Associated Erosion (m/year) (Trosclair, 2013)
1	23.3	3.2–3.3	0.9
2	7.1	2.4–2.7	0.3
3	0.9	2.1–2.5	0.07
4	0.7	2.1–2.5	0.06
5	0.5	2.1–2.5	0.05
6	0.8	2.1–2.5	0.06

required to build the terracing continues to increase past a certain length, the amount of reduction created begins to decrease. Fig. 9 shows this trend as the points in the scatter plot follow a logarithmic-type curve. Here the various colors represent observation points 2–9 and the symbols represent the configuration. Configuration 1, without any terracing, is considered the base example, so the reduction and length are both 0. The vertical line at 2000 m represents the length of shoreline protected by the terracing. The benefits gained from adding more terrace length begin to decrease after about 4 600 m. The trendline, shaded in grey, shows the average trend for all observation points within the plot.

4.2. Deposition results

For this analysis, bed shear stress is used as an indicator for depositional and erosional processes. During the two-week simulation period,

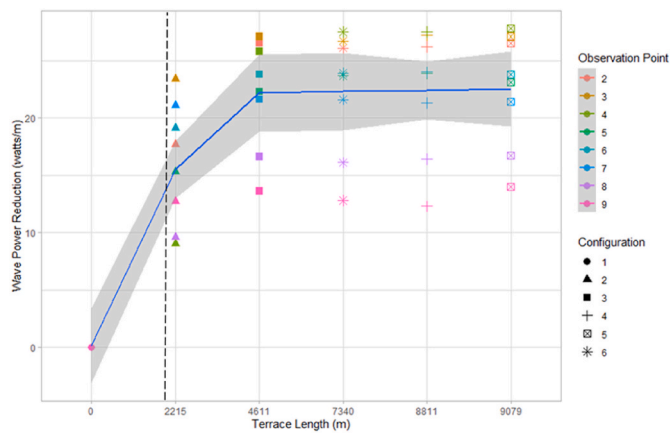


Fig. 9. Terrace Length versus Wave Power Reduction. The wave power reduction in watts/m per length in m of terrace required is shown in the above plot. The vertical dotted line at 2000m represents the length of coastline the terraces cover. Most reduction happens within the first 4 600 m of terracing with the curve plateauing after. The scatter plot is colored by observation points (1–9) and symbolled by configuration (1–6).

the bed shear stresses throughout the entire flow domain ranged from 0 to 3.4 Pa. For the calculation of total depositional area, the bed shear stresses examined within this study included an area of 3,341,700 m² encompassing the terrace configurations within Little Vermilion Bay. The bed shear stress maps for the chosen threshold of 0.15 Pa are shown in Fig. 10 below, and the maps for thresholds of 0.20 Pa and 0.25 Pa are shown in Appendix C. Each dot within the map represents a grid cell within the model. A bed stress of 0 Pa is represented by blue and includes the land area which will not experience bed shear stress by water except during high floods. A bed shear stress of 0.15 Pa and greater is displayed by the salmon color in the maps. This is the shear stress that is assumed to be conducive to erosion of silt in this study. Anything between 0 Pa and 0.15 Pa is represented by the gradient of colors and is considered to be the “depositional zone”. The silt DAR is also given for each configuration in Fig. 10.

Configuration 1 represents the as-built terrace configuration, and these results predict the sediment patterns produced thereby. The bed shear stress map shows higher shear stresses, represented in salmon, along the southwest-northeast terraces perpendicular to the canal. High shear stresses are also present in the north extent of the configuration, adjacent to the canal, and at the southern extent near the bay. Finally, there is areas of low bed shear stress within the terrace berms, represented in blue. This predicted pattern is corroborated by satellite imagery and field visit reports which give similar accounts. The higher shear stresses along the terrace berms represent channel formations. The higher bed frictions near the northern and southern extents describe the erosional processes occurring within the project at the flow inlet and near the open bay. Finally, extensive mudflat development was recorded within terrace sets in a pattern similar to that of the low shear stress patterns shown here.

Configuration 1 produced a DAR of 5.2, the second highest of all configurations. Most deposition occurred near and within the terrace berms. Erosional patterns were observed in the conveyance channels between terrace units and parallel to northeast-southwest berms. Erosion was also present at the berms nearest Four Mile Canal and at the southern extent near the open bay. This configuration required a comparatively smaller amount of area to build, 234,000 m², and produced a large amount of depositional area, 1,218,400 m².

Configuration 2, which widened the terracing by 100%, resulted in a DAR of 2.3. The amount of area required to build this configuration significantly increased, doubling to 468,000 m². There was no significant change in depositional area created. This resulted in the lowest DAR out of all configurations. The depositional pattern follows a similar path

as Configuration 1.

The highest ratio was produced by the delta-splay configuration (Configuration 3), which produced a silt DAR of 9.0. This configuration required the least amount of area to build, 160,600 m², and produced the highest amount of silt depositional area, 1,441,800 m². The area of deposition appears to accumulate behind the terrace berms, opposite the river input from Four Mile Canal, and within borrow pits. Notably, there is sufficient deposition that extends beyond the terrace berms compared to other configurations.

Configuration 4, the grid configuration, produced a DAR of 4.2. The depositional pattern shows that sediment accumulations are again favorable near the southern extent of terracing, furthest from the flow input from the Vermilion River and Four Mile Canal. There is also noticeable deposition within the borrow pit areas of the configuration.

Configuration 5, which included circular terracing, gave a DAR of 3.0. The area required to build the terracing is relatively high, 326,725 m², and the depositional area created is comparable to previous scenarios. Deposition was present mostly inside of terrace circles and in some areas near the southern extent of the configuration.

Finally, Configuration 6 simulated a chevron configuration, which was previously hypothesized to be a preferred configuration for wave energy attenuation and sediment deposition. This configuration received a DAR of 3.1. The depositional pattern shows a favorable amount of accumulation within the chevron configuration and near the berms but does not show much deposition outside of the configuration. Again, depositional areas are present near the south-southwestern extent of the configuration and within excavation pits.

Due to uncertainty associated with estuarine sediment dynamics, the exact numbers produced by the model are not precisely equivalent to the amount of depositional area that will be produced by a configuration. However, the trends and quantities estimated here are useful when considering future project designs. Table 5 summarizes the area of deposition, area of terracing, and DAR for all of the chosen silt thresholds, including 0.15 Pa, 0.20 Pa, and 0.25 Pa. The area of deposition increases, and subsequently the DAR, as the threshold for erosion increases. The ranking of each configuration remains the same, but each configuration’s depositional efficacy is not linearly related to grain size. For example, by increasing the threshold to 0.20, the DAR of Configuration 1 increases by 2.7 (52%), while the DAR of Configuration 4 increases by 1.8 (43%).

5. Discussion

By comparing the outputs of each model simulation, a few key insights can be made about terrace design parameters. Wave power reduction experienced at the leeward shoreline is dependent upon the length of terracing added, the main wind direction, and the configuration chosen. It is notable in this study that after a certain terrace length, the efficacy of wave power reduction begins to decrease. At this specific site, that length is around 4600 m, about twice the length of protected shoreline. Some of this plateauing is purposeful, as extra terrace rows act as sacrificial berms protecting following rows. This allows a period of time for progradation and vegetation, through deposition behind berms, to occur before the berms are susceptible to wave attack. This concept was supported by depositional patterns present during a site visit to Little White Lake. The first row of terracing had begun to grow into the neighboring shoreline, effectively adding marsh land and extending the shoreline. The outer rows open to wave attack were eroded but provided enough attenuation and time for leeward rows to prograde. More information about the details of this site visit can be found in Appendix D. After this effective length of constructed protection, the configuration chosen begins to matter less. Configurations 3–6 produce similar reduction percentages, with small variations across observation points.

The main wind direction which produced increased wave power along the Little White Lake shoreline was between 100° and 200°. To form waves capable of eroding marsh edge common to Louisiana, there

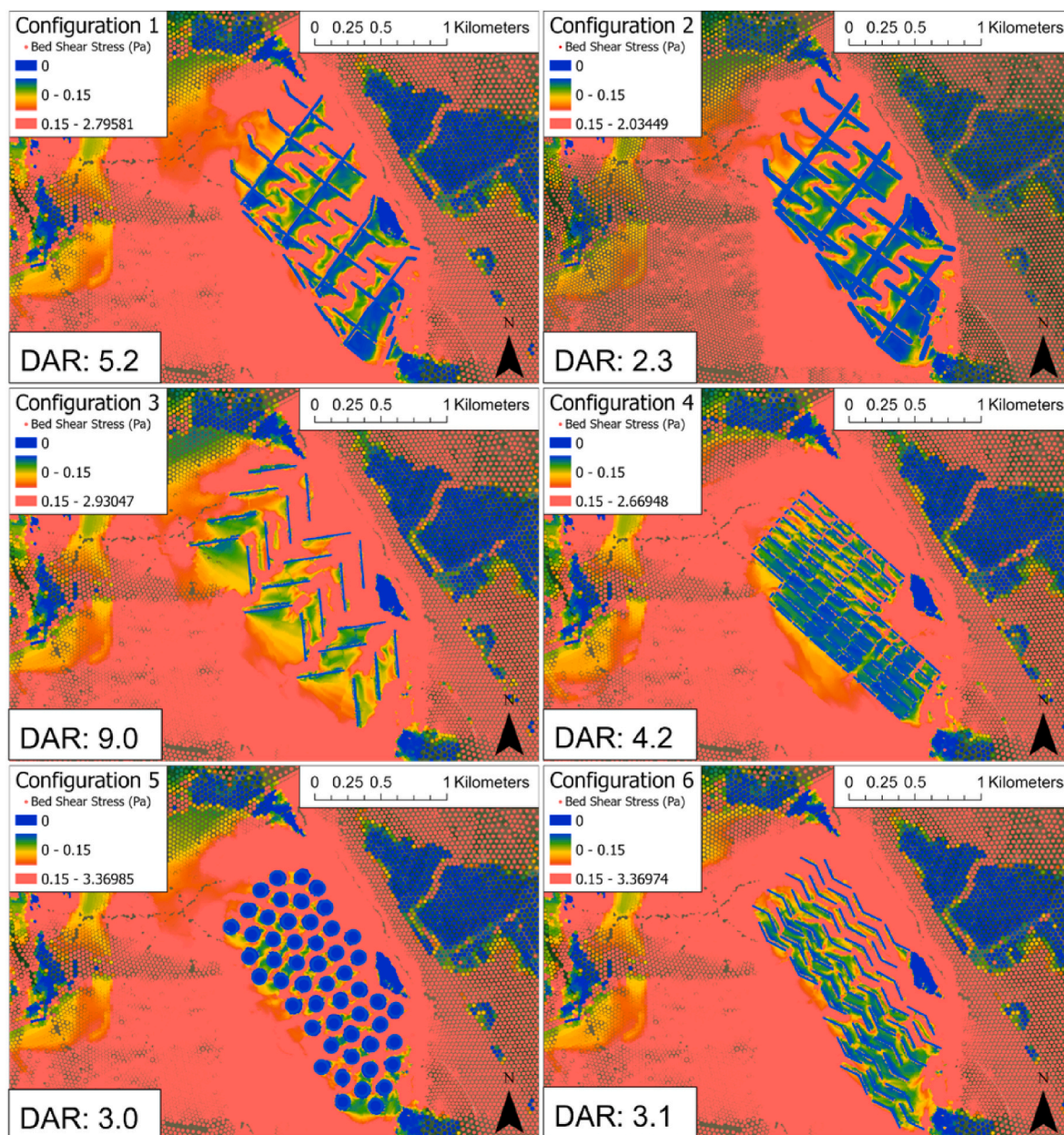


Fig. 10. Silt Bed Shear Stress Patterns. Bed shear stresses for each of the six configurations were mapped and the DAR was calculated. Each dot represents a grid cell, and the color represents the highest bed shear stress experience on that cell over the entire simulation period. Here, 0.15 Pa is assumed to be the threshold for erosion of silt and visualized in salmon. Any other color represents the gradation of bed shear stresses below that threshold, assumed to be depositional.

must be approximately four km or more of uninterrupted wave fetch, and these angles meet that threshold distance here before reaching the coast (Allison et al., 2017). The observation points which received the greatest wave power reduction were located behind the berms that were placed perpendicular to the predominant wind direction. For example, observation point 7 had an average wave power throughout the storm event of 21.7 W/m without any terracing present (Configuration 1). By adding one linear row of terracing (Configuration 2), the wave power was reduced to 0.6 W/m, resulting in a 97% reduction. This concept was concluded in previous terracing studies and is once again confirmed here. However, the theory that suggested a chevron configuration to be the most effective at attenuating wave energy and inducing deposition was not substantiated in this study. This is most likely due to the shape of the embayment, which effectively blocks wind fetch at directions ranging from roughly 90°–200°. Although the chevron shape (Configuration 6) sufficiently decreased wave power, it did not do so any more

advantageously than other configurations at similar lengths.

Another important concept was realized through the wave power analysis of Configuration 4. This scenario, which included all linear terraces and the individual berms in the center of Little White Lake, actually created more wave power along the shoreline than the outputs from the removal of the extra individual berms (Configuration 4, part 2). As the individual terrace berms effectively blocked the natural wave-current path, they also accelerated velocities at berm edges as flow was forced around the berms. The slanted terraces were originally placed to help capture sediment-laden flow from the adjacent channel, but, instead, they pushed flow and wave energy around and behind the protective linear terraces. A snapshot in time of this wave energy channelization can be seen in Appendix B. Under these conditions, an increase in terrace length, and subsequently cost, decreased the efficacy of the configuration to reduce wave power. Modeling prior to project implementation can remove the detrimental effects of unconsidered

Table 5

DAR Calculations. DAR was calculated for each configuration by dividing the depositional area by the terrace area. The table shows the depositional area and DAR for a bed shear stress threshold of 0.15 Pa, 0.20 Pa, and 0.25 Pa.

Little Vermilion Bay					
0.15 Pa Threshold					
Simulation	Width (m)	Terrace Length (m)	Terrace Area (m ²)	Silt Depositional Area (m ²)	DAR
Configuration 1	20	11,700	234,000	1,218,400	5.2
Configuration 2	40	11,700	468,000	1,072,900	2.3
Configuration 3	20	8030	160,600	1,441,800	9.0
Configuration 4	20	14,630	292,600	1,217,700	4.2
Configuration 5	20	16,336	326,725	1,121,875	3.0
Configuration 6	20	14,570	291,400	903,300	3.1
0.20 Pa Threshold					
Configuration 1	20	11,700	234,000	2,081,400	7.9
Configuration 2	40	11,700	468,000	2,166,700	3.6
Configuration 3	20	8030	160,600	2,044,400	11.7
Configuration 4	20	14,630	292,600	2,046,900	6.0
Configuration 5	20	16,336	326,725	2,075,700	5.4
Configuration 6	20	14,570	291,400	1,959,700	5.7
0.25 Pa Threshold					
Configuration 1	20	11,700	234,000	2,375,300	9.1
Configuration 2	40	11,700	468,000	2,485,800	4.3
Configuration 3	20	8030	160,600	2,291,500	13.3
Configuration 4	20	14,630	292,600	2,472,500	7.5
Configuration 5	20	16,336	326,725	2,342,900	6.2
Configuration 6	20	14,570	291,400	2,301,300	6.9

terrace elements and allocate project funding more appropriately.

Marsh edge erosion by wave action is a known primary driver of shoreline retreat within coastal wetlands (Allison et al., 2017). In this study, the wave power outputs were related to shoreline erosion using previously established empirical equations. By doing so, the potential marsh protected by each configuration could also be quantified. The contour of the shoreline, wind and wave direction and magnitude, and necessary length of terrace protection will inherently vary from site to site. However, the methods presented in this study of quantifying wave power at the shoreline, comparing terrace length to the amount of wave power reduction, and quantifying potential protected shoreline through numerical modeling can be applied at any future terracing project. This can save costs through the reduction of terrace length required for the same or an increased performance of wave power attenuation, achieving an optimal configuration for slowing marsh edge retreat.

There is no trend found between terrace area constructed and produced depositional area; rather, the amount of land presumably produced is dependent on the shape of the configuration and its ability to disrupt the wind-wave-current pattern. The absence of increase in the silt deposition ratio between Configuration 1 and Configuration 2 suggests that the widening of terraces does not produce a depositional area gain commensurate to the amount of land required to build the project. While the area required to construct the configuration increased by

100%, the depositional area did not increase correspondingly.

The optimal configuration for this site was determined to be the delta-splay configuration (Configuration 3), which received the highest DAR. Not only did this configuration create the greatest amount of depositional area, but it also required substantially less area to construct it. This finding is corroborated by the outcome of nearby delta-like terrace designs, such as TV-12 Little Vermilion Bay Sediment Trapping Project, which have fared particularly well (McGinnis, personal communication, 2021; Castellanos and Aucoin, 2004). Turner and Streever (2002) also spoke on the status of TV-12 attributing its success to open communication lines between agencies, contractors, and stakeholders, adequate investigation of sediment conditions prior to construction, consideration of berm consolidation, and project timing and scheduling. The outcome of this configuration suggests a positive relationship between the delta shape and sediment deposition. Like a real delta, the feeder channels are able to successfully direct flows in a variety of directions, block high wind and wave energy in depositional areas, and spread sediment throughout. Interestingly, the delta-splay configuration is also most effective at reducing bed shear stresses and presumably influencing sedimentation at the greatest distances away from the terrace berms.

The depositional pattern changes from configuration to configuration, but deposition was favored within and near the berms of terrace projects. This suggests that the terracing is effectively altering the path of sediment-laden flow. Deposition, through lowered bed shear stress, is favorable at the southern and southwestern extent of the configuration. This is likely related to the higher extent of hydrologic connectivity found in the configuration closest to the flow source (Four Mile Canal) versus the intermediate connectivity within the south-southwest portion. High flow connectivity has the ability to wash sediment through and out of its system, while low to intermediate hydrologic connectivity is conducive to sediment trapping (Matthews, 2020). Furthermore, erosional areas are often present along the edges of individual terrace berms. This similar depositional pattern was concluded in previous works that found increased water velocities and bed shear stresses occurring as water is forced around an impermeable surface. Some distance downstream of the terraces, the velocities settle back into their natural flow path, but the terrace effectively creates a protected depositional zone directly behind the terrace and an increased erosive zone at terrace edges (Matthews, 2020).

Finally, sediment trapping is favored within the lowest subaqueous areas in the configuration, the excavation pit. This is another idea that has been proven directly through feldspar sampling for sediment accretion within terrace configurations and is now proven through numerical modeling. Sediments tend to accumulate within the lowest depths to reduce bathymetric irregularities within the bottom surface. However, the concept that this accumulation will lead to mudflat creation and land emergence is not yet certain.

Further studies that will reduce the uncertainties underlying the efficacy of marsh terracing should include morphological modeling components and the analysis of their performance under storm surge. Doing so would allow for an analysis of erosional and depositional patterns over time. The analyses within this study were reflective of the as-built terrace configurations, without the effects of consolidation, erosion, deposition, and sediment movement. As terrace berms are eroded, their efficacy for wave power reduction and deposition will also be reduced. Conversely, as terraces consolidate, prograde, and vegetate, their efficacy to attenuate wave energy and influence deposition will increase. Storm surge is a major contributor to sediment dynamics within the Northern Gulf of Mexico, and only the effects of localized wind events were examined in this study. By analyzing terrace performance under storm surge, their susceptibility to tropical storm events could be analyzed. This analysis can also be addressed through the use of numerical modeling.

Furthermore, an increase in post-project monitoring would greatly increase model capabilities and allow for in-depth model validation.

Monitoring recommendations include cross-sectional surveys of terrace bathymetries, velocity gauges, and wave gauges. Surveys of the terraces at regular intervals would allow for a sediment budget of marsh land gain versus loss. Depths at excavation pits and between terraces could quantify the sediment accretion within the project, while depths at berms and near terrace edges could quantify any losses. This project did not have a velocity gauge installed, and the validation of flow patterns within the model domain relied on the analysis of salinity fluctuations. Velocity readings would provide a superior method to calibrating model circulation dynamics. Finally, establishment of wave gauges along the shoreline could further verify that the wave power calculations are accurate.

Currently, terracing efforts are limited to those constructed within the Northern Gulf of Mexico, but the idea could potentially be implemented to other regions with similar estuarine conditions. Results at different sites will vary as they are dependent on various factors including marsh geometry, soil characteristics, suspended sediment load, meteorological conditions, and hydrology. However, the methodology of modeling and the post-processing tools used here can be utilized prior to terrace constructions in the future to find the optimal configuration for a specific site. These numerical tools can help resource managers evaluate different configurations, quantitatively assess performances, and define the outcomes of sediment transport, wave power, or both. Doing so is less costly than field experiments and could potentially increase the amount of terrace projects implemented in Louisiana and along other coasts.

6. Conclusion

Marsh terracing as a restoration technique has been implemented for over 30 years along the Louisiana coast, but few studies have attempted to evaluate their hydrodynamic performance. Terraces have been proven to create additional marsh edge and subsequently create a heap of ecological benefits, such as increasing estuarine biomass and providing habitat to endangered waterbird species. However, the lack of hydrodynamic performances assessments has led to costly and time-consuming experimental project design plans and implementation of sub-optimal configurations for the local flow and wave dynamics of specific sites.

This study sought to quantify the magnitude of wave energy reduction and sediment deposition due to terracing and create a set of performance metrics to evaluate future terrace projects prior to implementation. This was completed through the development and calibration of a high resolution, two-dimensional hydrodynamic numerical model on Delft3D Flexible Mesh. The unstructured grid capabilities of the model allowed for outputs at a highly refined spatial scale. The wave modeling capabilities of D-Wave allowed for calculations of wave propagation, generation by wind, dissipation, and the communication of those outputs with D-Flow. Because of its high-resolution flow and wave modeling capabilities, open-source code, and ability to reproduce the relevant processes, the use of Delft 3D is suggested for terrace design studies.

The magnitude of wave energy reduction was quantified through a set of calculations that were a function of wave height, wave period, and relevant outputs from the model, followed by the creation of a wave power time series for multiple observation points along the coast. The reduction was related to the linear length of terrace required by creating a scatter plot of length versus wave power reduction. Once this metric was established, six different configurations were comparatively assessed for their ability to decrease wave energy along a shoreline.

The magnitude of deposition was quantified by selecting a threshold for which particle erosion would occur and comparing that threshold to the bed shear stress outputs experienced in each cell of the model. The area below the selected threshold was related to the area required to construct the terraces through the creation of the Deposition Area Ratio (DAR) metric. Similarly, to show the utility of this tool, the ability of six

different configurations to induce sediment deposition and create emergent marsh were comparatively assessed.

If marsh terracing restoration projects are to be implemented in the future, their benefits must be quantified. The use of these metrics is a simple way to evaluate the benefits of marsh terracing, wave energy reduction and land gain, along with the effort required for project implementation, labor and costs. The methodology established in this study offers a numerical tool to aid resource managers in quantifying performance-based outcomes at their specific study site. While local flow and wave conditions are site specific, this tool was successfully applied, and a few outcomes about the Vermilion Bay terracing project were discovered through it.

- (1) The effectiveness of a terrace configuration to attenuate wave energy was dependent upon the length of terraces constructed. The length of coastline protected by the terraces was 2000 m. After about double that length, 4600 m, the ability for the configuration to continue to attenuate wave energy decreased. After the effective length, all configurations performed relatively the same, at nearly 100% reduction. While some of this plateauing is purposeful, through the creation of sacrificial terraces, continuing to add more terraces well past this effective length might not be a beneficial use of project funds and effort.
- (2) The individual extra berms within the center of Little White Lake were determined by the model to have detrimental effects on wave attenuation. The configuration without these terraces attenuates wave power more effectively than the configuration with the individual center berms. The extra terracing channelized wave energy behind the berms and closer to the shoreline. This negative effect further supports the use of numerical modeling and performance metric analysis prior to project implementation.
- (3) Terrace widening did not produce an additional land area commensurate to the amount of land necessary to construct the configuration. Terrace widening without prior analysis may lead to increased construction costs with little gain in benefits.
- (4) The delta-splay configuration was deemed the optimal configuration for Little Vermilion Bay, though this recommendation is not universal. The delta-like form seems to imitate a natural delta, effectively slowing velocities and spreading sediment. This conclusion was also corroborated by the success of the neighboring delta-splay terrace project. It also required significantly less land to build this configuration, which yielded a high DAR.

Overall, the conclusions established here are specific to the model domain, the Vermilion Bay Four Mile Canal Terracing and Sediment Trapping project. However, the tools and methods presented here can be used universally to determine the optimal terrace configuration for a specific site. Doing so increases stakeholder and public involvement, ensures the most advantageous use of project funding, and advances the implementation of marsh terracing as a coastal restoration technique. Further research should include morphology aspects within the modeling effort, storm surge analysis, and further establishment of post-project monitoring. All potential future studies can be analyzed and built upon by utilizing the numerical modeling methods and performance metrics presented herein at various terrace project sites.

Funding

This work was partially supported by the Louisiana Sea Grant program, Louisiana State University, Baton Rouge, LA.

CRedit authorship contribution statement

Katelyn A. Keller: Methodology, Validation, Formal analysis, Writing, Visualization. **Kelin Hu:** Conceptualization, Methodology, Software, Supervision. **Ehab A. Meselhe:** Conceptualization,

Methodology, Software, Supervision, Funding acquisition.

Declaration of competing interest

The authors declare that they have no known competing financial interests or personal relationships that could have appeared to influence the work reported in this paper.

Acknowledgements

The authors would like to acknowledge Dr. Mead Allison and Dr. Nicole Gasparini of Tulane University for providing advice and

assistance throughout the development process and for the final proof reading of the article. They would also like to acknowledge Tommy McGinnis and Bernard Wood of the Coastal Protection Restoration and Authority Lafayette Regional Office for providing a field visit to and communications about the Vermilion Bay terracing projects. Finally, they would like to provide acknowledgement to Dr. Robert Twilley at Louisiana State University for organizing the funding for this project. This research was completed, in part, by using high-performance computing (HPC) resources and services provided by both the Louisiana Optical Network Infrastructure (LONI) and Technology Services at Tulane University.

Appendix A. Boundary Time Series Graphs

There were five open boundaries within the flow model and spatially uniform wind data imposed over the entire domain. The time series in this appendix shows the time series for all open boundaries within the flow model acquired from their respective stations. Each graph is plotted from June 1, 2019 to December 1, 2019 to capture both the flow calibration period and the model simulation period. There are two periods highlighted in each graph. The first highlighted grey box ranges from June 1, 2019 0:00 to July 1, 2019 0:00 and represents the flow calibration period. The second grey box highlights the model simulation period ranging from October 1, 2019 0:00 to October 14, 2019 0:00. The wind event examined during the wave power analysis which ranged from October 9, 2019, 12:00 to October 11, 2019 12:00 is also presented in its own graph here for further insights.

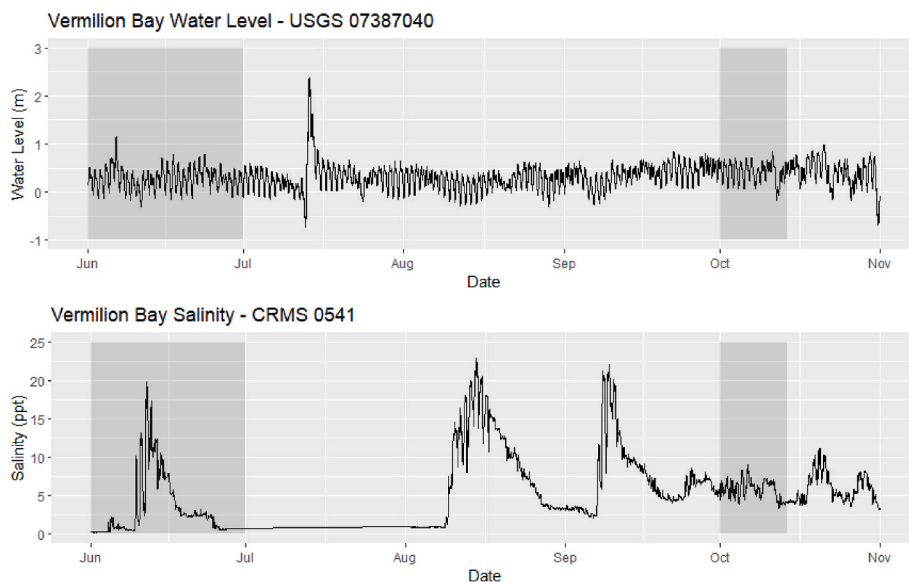


Fig. A1. Water level and salinity conditions imposed at the Vermilion Bay boundary. Note that salinity levels range between 0 ppt and 20 ppt during the calibration period.

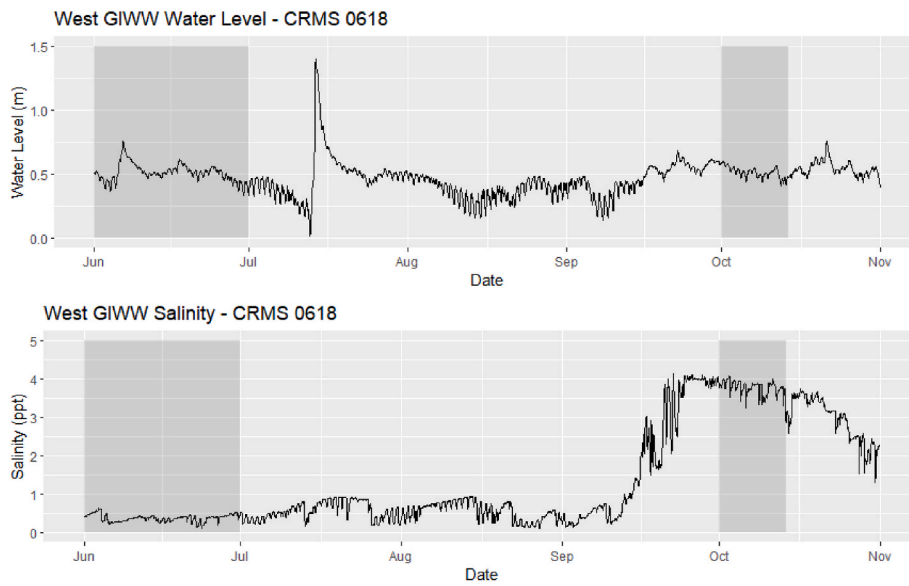


Fig. A2. Water level and salinity conditions imposed at the Western Gulf Intracoastal Waterway (GIWW) boundary.

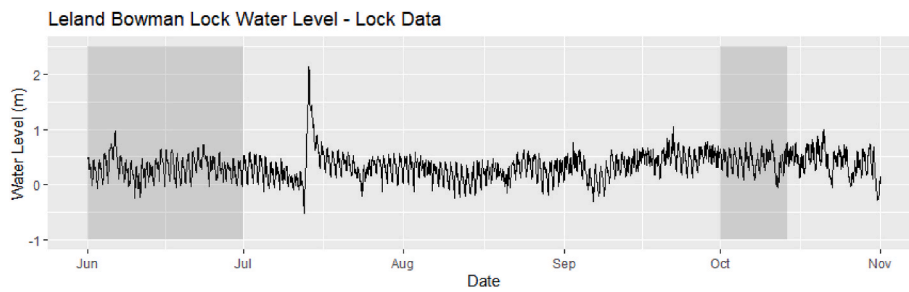


Fig. A3. Water Level conditions imposed at the Leland-Bowman Lock Boundary.

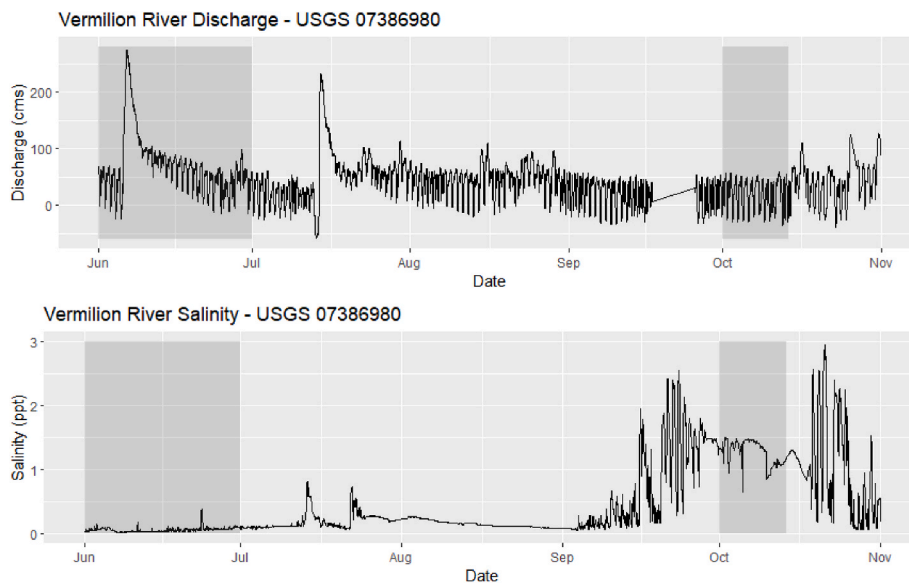


Fig. A4. Discharge and salinity imposed at the Vermilion River boundary. Note that discharges have a wide range, from 0 cms to 275 cms.

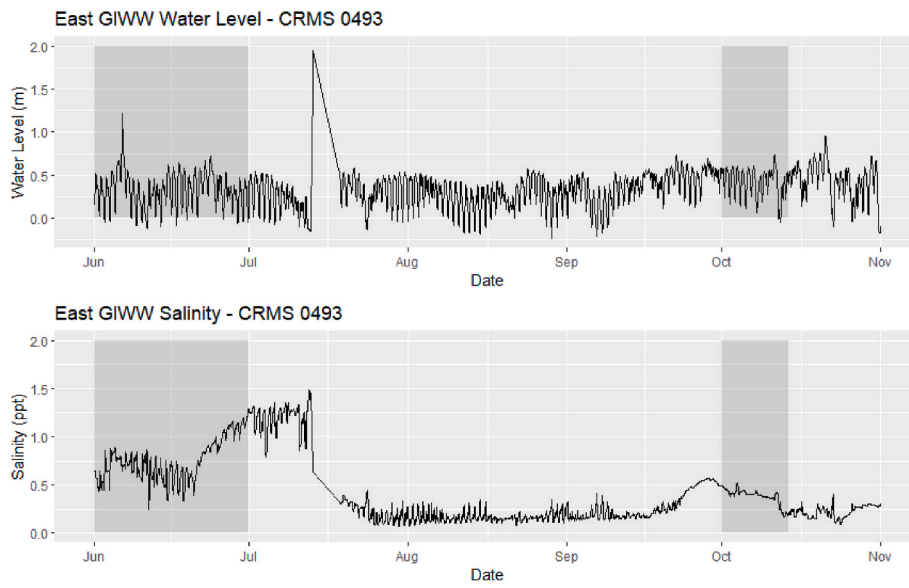


Fig. A5. Water level and salinity imposed at the Eastern Gulf Intracoastal Waterway boundary.

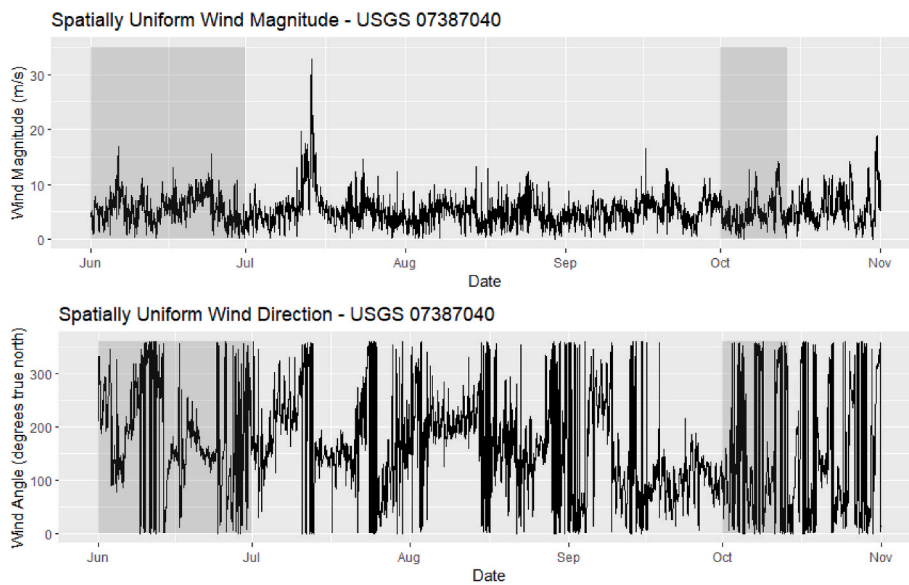


Fig. A6. Spatially uniform wind magnitude and direction applied over the entire flow grid.

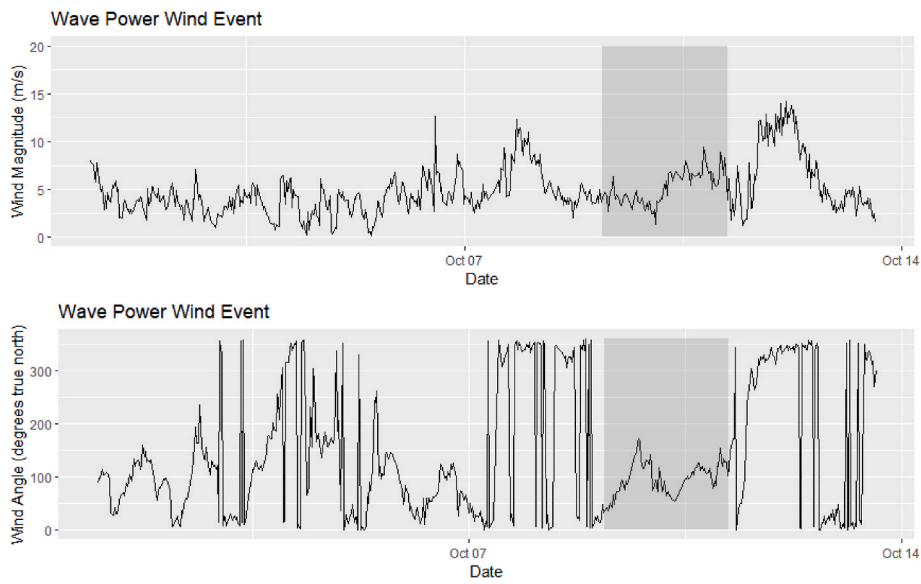


Fig. A7. Highlighted in grey is the localized wind event examined during the wave power analysis. Note that the angles fell within the optimal period for wave propagation at the chosen observation points due to the alignment of the Little White Lake shoreline ($\sim 100^\circ\text{--}200^\circ$).

Appendix B. Wave Power Supplementary Material

A total of 12 observation points were placed along the Little White Lake shoreline to create plots of wave power over time. The wave power reduction seen at each observation point differs slightly depending on its location relative to a terrace berm. The colors represent the six different configurations.

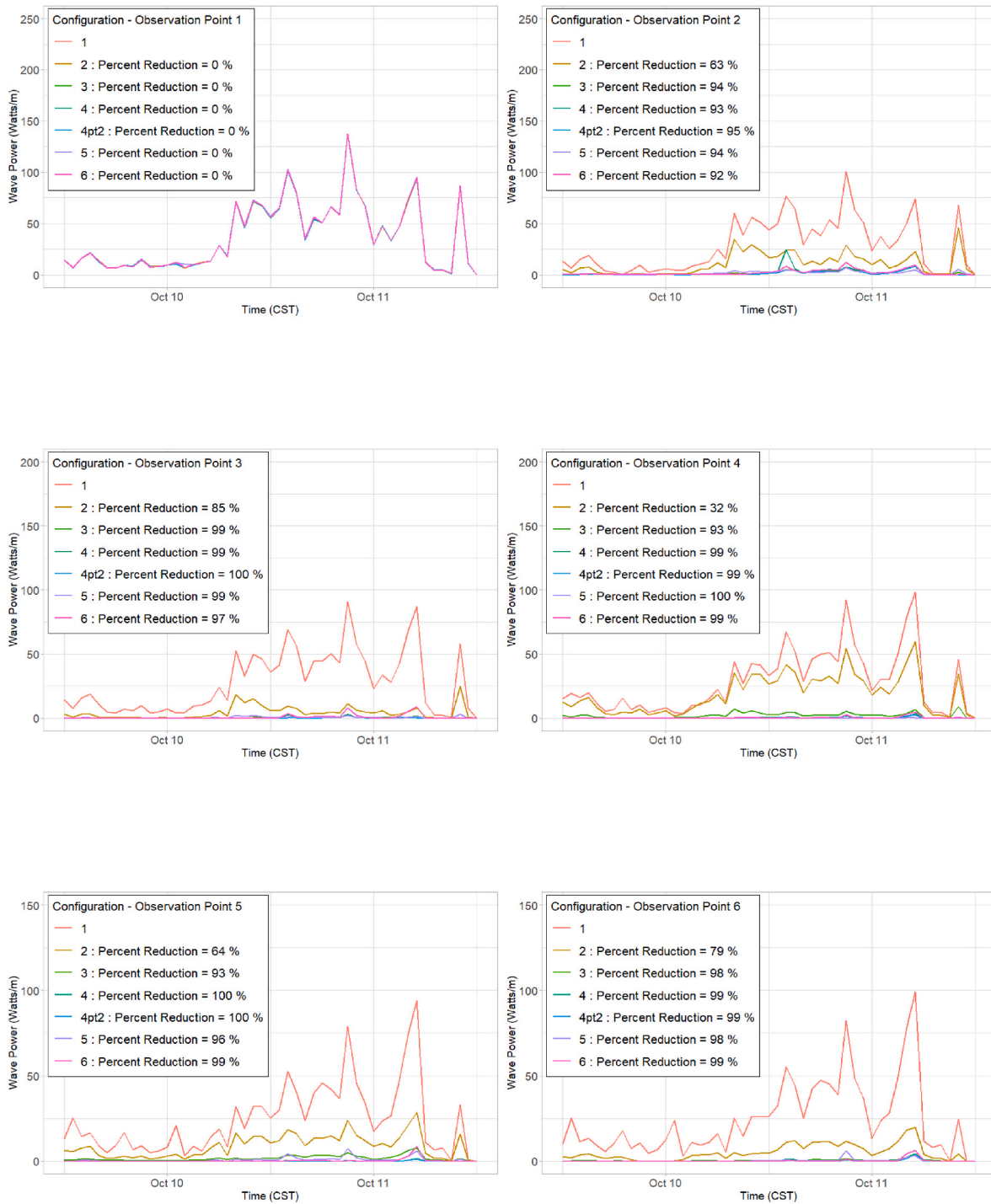


Fig. B1. Wave power time series and reduction analysis at all 12 observation points.

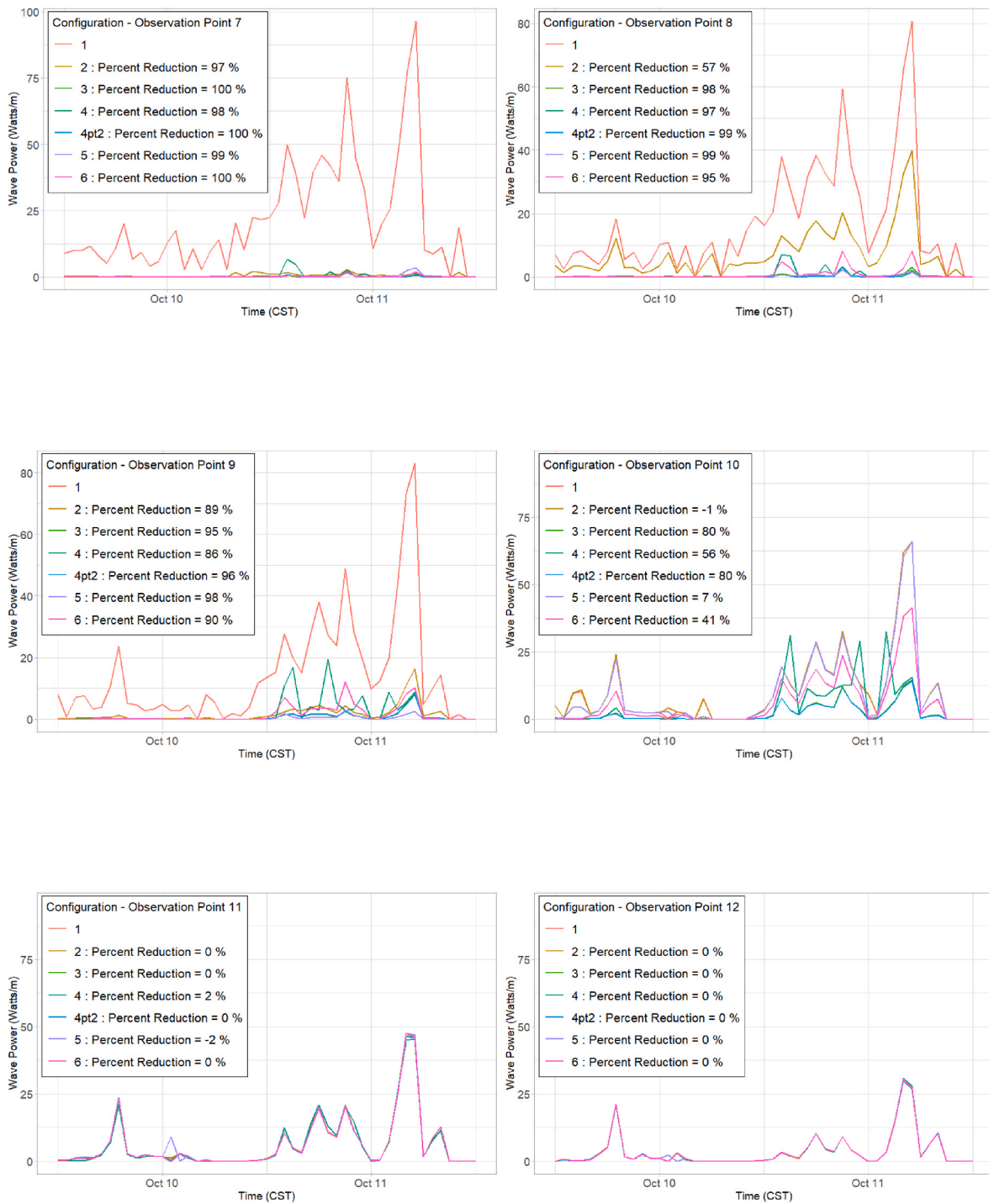


Fig. B1. (continued).

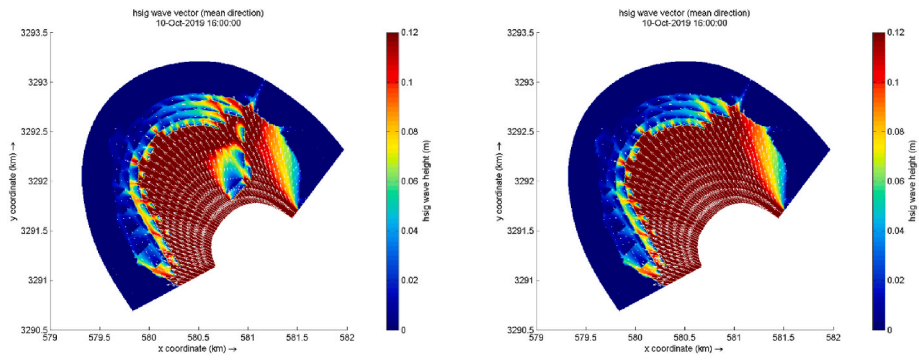


Fig. B2. Wave event occurring on 10-Oct-2019 16:00:00. The presence of the individual berms in the center of Little White Lake (left) is increasing wave heights on the Northeastern side of the linear terrace configuration. Without the berms (right) wave heights near that area are decreased. Here, the colors represent wave height, and the arrows represent mean wave direction.

Appendix C. Deposition Supplementary Material

The depositional maps for erosion thresholds of 0.20 Pa and 0.25 Pa are shown in this section.

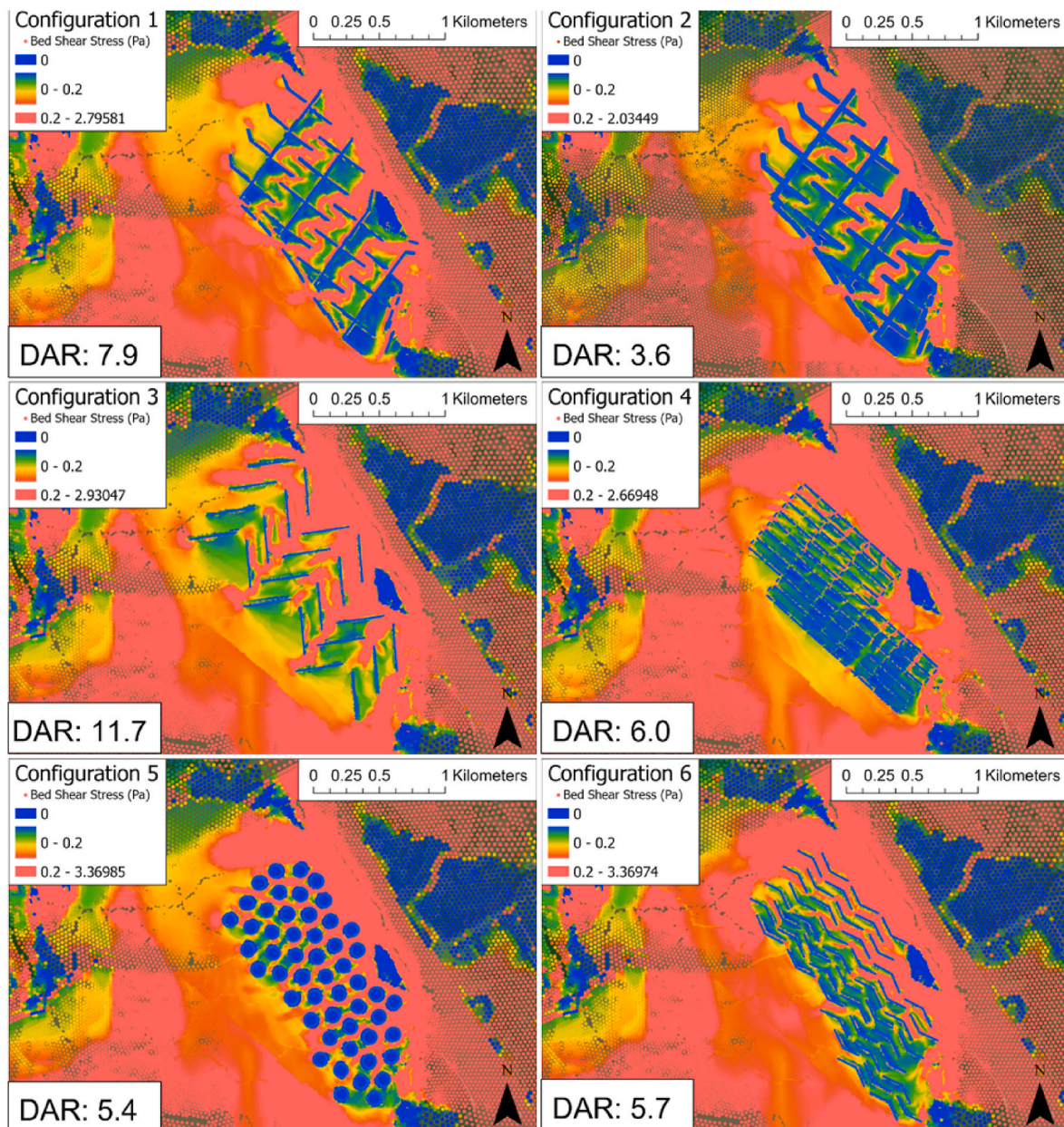


Fig. C1. Depositional Pattern with a 0.20 Pa Bed Shear Stress Threshold. Bed shear stresses for each of the six configurations were mapped and the DAR was calculated. Each dot represents a grid cell, and the color represents the highest bed shear stress experience on that cell over the entire simulation period. Here, 0.20 Pa is assumed to be the threshold for erosion of silt and visualized in salmon. Any other color represents the gradation of bed shear stresses below that threshold, assumed to be depositional.

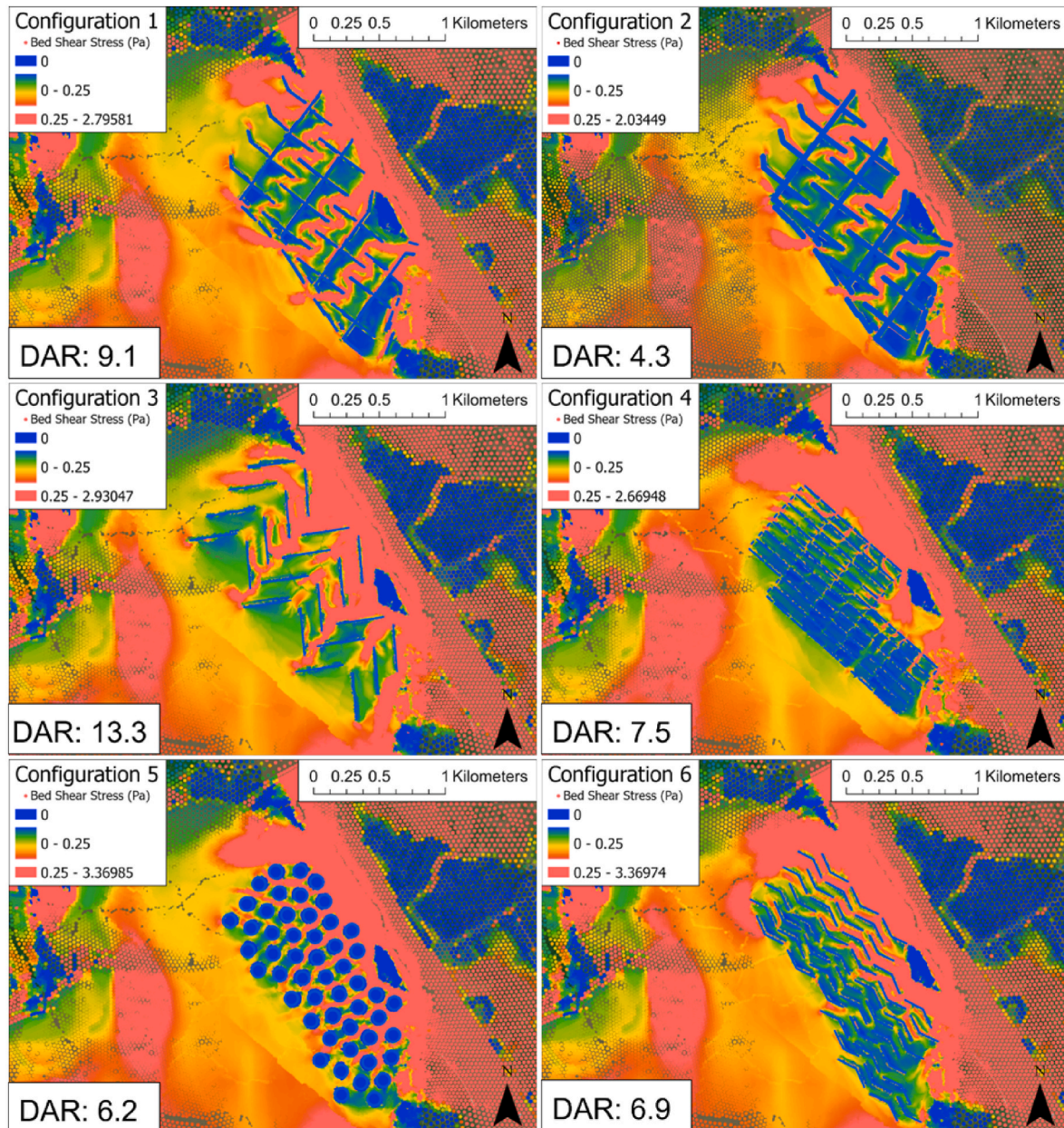


Fig. C2. Depositional Pattern with a 0.25 Pa Bed Shear Stress Threshold. Bed shear stresses for each of the six configurations were mapped and the DAR was calculated. Each dot represents a grid cell, and the color represents the highest bed shear stress experience on that cell over the entire simulation period. Here, 0.25 Pa is assumed to be the threshold for erosion of silt and visualized in salmon. Any other color represents the gradation of bed shear stresses below that threshold, assumed to be depositional.

Appendix D. Site Visit

A site visit to Vermilion Bay terracing was completed August 18, 2021. CPRA employees, Tommy McGinnis and Bernard Wood, drove the airboat around TV-18 Four Mile Canal Terracing and Sediment Trapping and TV-12 Little Vermilion Bay Sediment Trapping. The site visit gave a good account of the current state of both terrace configurations. The outer two rows of linear terraces within Little White Lake, those most susceptible to wind and wake energy, were mostly submerged or completely eroded away. The inner rows have grown together and into the shoreline. More sediment deposition and mudflat accumulation was found near the eastern adjacent channel, with less sediment flow carried westward. Within the fishnet terraces of Little Vermilion Bay, a few morphological patterns were noticed. First, there was a clear channelization on the leeward side of NE-SW berms. Second, there was heavy erosion in the terraces nearest to Four Mile Canal and those at the south extent of the configuration. Finally, extensive mudflat deposition was present in between berms. The TV-12 terraces within Little Vermilion Bay fared extremely well, which McGinnis attributes to its delta-like configuration. Plenty of native vegetation is found within the configuration. The main calibration station used within this study, CRMS 2041, was also located and stage measurements collected.



Fig. D1. CRMS 2041 Gage Location. On the site visit, we were able to view the location of our main calibration station, CRMS 2041, to get an idea of its conditions.



Fig. D2. Visible erosion was present along the terrace edges from wave attack and current erosion. The scalloped nature of the shoreline (left) gives an idea of how the main wind and wave direction erodes away sediment and moves it along in a path parallel to the terrace. Current driven erosion (right) cuts much deeper, causing vegetation to fall into the water without any structural support underneath.

References

- Allison, M., Chen, Q.J., Couvillion, B., Freeman, A., Leadon, M., McCorquodale, A., Meselhe, E., Ramatchandirane, C., Reed, D., White, E., 2017. 2017 Coastal Master Plan: Model Improvement Plan, Attachment C3-2: Marsh Edge Erosion. Version Final. Coastal Protection and Restoration Authority, Baton Rouge, Louisiana, pp. 1–51.
- Aucoin, Associates, 2004. Four-Mile Canal Terracing and Sediment Trapping Project (TV-18) (AS-BUILT). Louisiana Department of Natural Resources, Coastal Restoration Division, Lafayette, Louisiana, USA.
- Balkum, K., Belhadjali, K., Cowan, J., Stead, M., 2003. East Sabin Lake Hydrologic Restoration, Construction Unit 1 (CS-32 Ecological Review. Louisiana Department of Natural Resources, Coastal Restoration Division, Lafayette, Louisiana, USA.
- Baustian, M., Meselhe, E., Jung, H., Sadid, K., Duke-Sylvester, S., Visser, J., Allison, M., Moss, L., Ramatchandirane, C., Sebastiaan van Maren, D., Jeuken, M., Bargu, S., 2018. Development of an Integrated Biophysical Model to represent morphological and ecological processes in a changing deltaic and coastal ecosystem. *Environ. Model. Software* 109, 402–419.
- Brasher, M.G., 2015. Review of the Benefits of Marsh Terraces in the Northern Gulf of Mexico. Ducks Unlimited, Inc., Gulf Coast Joint Venture, Lafayette, LA, USA.
- Castellanos, D., 2003. Little Vermilion Bay Sediment Trapping (TV-12) Summary Data and Graphics. Louisiana Department of Natural Resources, Coastal Restoration Division, Lafayette, Louisiana, USA.
- Castellanos, D., Aucoin, S., 2004. 2004 Operations, Maintenance and Monitoring Report for Little Vermilion Bay Sediment Trapping (TV-12). Louisiana Department of Natural Resources, Coastal Restoration Division, Lafayette, Louisiana, USA.
- Coastal Protection and Restoration Authority of Louisiana, 2017. Louisiana's Comprehensive Master Plan for a Sustainable Coast. Coastal Protection and Restoration Authority of Louisiana (Baton Rouge, Louisiana, USA).
- Coastal Protection and Restoration Authority (CPRA) of Louisiana, 2022. Coastwide reference monitoring system-wetlands monitoring data. Retrieved from Coastal Information Management System (CIMS) database. <http://cims.coastal.louisiana.gov>
- Couvillion, B.R., Beck, H., Schoolmaster, D., Fischer, H., 2017. Land Area Change in Coastal Louisiana (1932 to 2016), vol. 3381. U.S. Geological Survey Scientific Investigations Map, p. 16p (pamphlet).
- Deltares, 2019a. D-flow Flexible Mesh User Manual. Deltares, Version 1.5.0.
- Deltares, 2019b. D-waves User Manual. Deltares, Version 1.2.
- French, J., 2020. Optimization of Marsh Terracing as a Wetland Restoration Technique: Mitigation of Cohesive Sediment Erosion by Waves Associated with Frontal Passage. Mississippi State University Master's Thesis.
- Guidry, M., Thibodeaux, C., 2004. 2004 Operations, Maintenance, and Monitoring Report for Pecan Island Terracing (ME-14). Louisiana Department of Natural Resources, Coastal Restoration Division, Lafayette, Louisiana, USA.
- Herman, Kernkamp, Dam, Arthur, Stelling, Guus, de Goede, Erik, 2011. Efficient scheme for the shallow water equations on unstructured grids with application to the Continental Shelf. *Ocean Dynam.* 61, 1175–1188. <https://doi.org/10.1007/s10236-011-0423-6>.
- Hersbach, H., Bell, B., Berrisford, P., Biavati, G., Horányi, A., Muñoz Sabater, J., Nicolas, J., Peubey, C., Radu, R., Rozum, I., Schepers, D., Simmons, A., Soci, C., Dee, D., Thépaut, J.-N., 2018. ERA5 Hourly Data on Single Levels from 1979 to Present. Copernicus Climate Change Service (C3S) Climate Data Store (CDS). <https://doi.org/10.24381/cds.adbb2d47>.
- Louisiana Coastal Wetlands Conservation and Restoration Task Force, 2017. Four Mile Canal Terracing and Sediment Trapping (TV-18) General Project Fact Sheet.
- Matthews, M., 2020. Geomorphic Effectiveness of Marsh Terracing as a Coastal Restoration Technique in Southern Louisiana. Tulane University Master's Thesis.
- Meselhe, E., Rodrigue, M., 2013. Models Performance Assessment Metrics and Uncertainty Analysis.
- Meselhe, E., Khalifa, A.M., Hu, K., Lewis, J., Tavakoly, A.A., 2022. Influence of key environmental drivers on the performance of sediment diversions. *Water* 14, 24. <https://doi.org/10.3390/w14010024>, 2022.
- Miller, M., Guidry, M., 2011. Operations, maintenance, and monitoring report for sweet lake/willow lake hydrologic restoration (CS-11b). In: Coastal Protection and Restoration Authority of Louisiana. Lafayette, Louisiana, USA.
- Osoorio, R., Linhoss, A., Dash, P., 2020. Evaluation of marsh terracing for wetland restoration: a remote sensing approach. *Water* 12 (2), 336.
- O'Brien, C., 2003. Jumbile Cove Restoration Project. Galveston Bay Estuary Program, West Bay, Galveston, Texas.
- O'Connell, J.L., Nyman, J.A., 2010. Marsh terraces in coastal Louisiana increase marsh edge and densities of waterbirds. *Wetlands* 30, 125–135.

- Parker, K.R., 2014. Field ND Numerical Investigation of Wave Power and Shoreline Retreat in Terrebonne Bay, Southern Louisiana, vol. 4125. LSU Master's Thesis.
- Ross, M.S., Mitchell-Bruker, S., Sah, J.P., et al., 2006. Interaction of hydrology and nutrient limitation in the Ridge and Slough landscape of the southern Everglades. *Hydrobiologia* 569, 37–59.
- Rozas, L.P., Minello, T.J., 2001. Marsh terracing as a wetland restoration tool for creating fishery habitat. *Wetlands* 21, 327–341.
- Sorenson, R.M., 2006. *Basic Coastal Engineering*. Springer.
- Swan, 2021. SWAN Scientific and Technical Documentation. SWAN Cycle III Version 41.31AB. Delft University of Technology, Netherlands.
- Temmerman, S., Meire, P., Bouma, T., Herman, P., Ysebaert, T., De Vriend, H., 2013. Ecosystem-based coastal defence in the face of global change. *Nature* 504, 79–83. <https://doi.org/10.1038/nature12859>.
- Thibodeaux, C., Grandy, G., Balkum, K., 2004. Four-mile canal terracing and sediment trapping (TV-18) monitoring plan. In: Coastal Protection and Restoration Authority of Louisiana. Lafayette, Louisiana, USA.
- Trosclair, K.J., 2013. Wave Transformation at a Saltmarsh Edge and Resulting Marsh Edge Erosion: Observations and Modeling. Department of Geological Sciences, University of New Orleans, New Orleans, La (Unpublished master's thesis).
- Turner, R.E., Streever, B., 2002. Approaches to Coastal Wetland Restoration: Northern Gulf of Mexico. SPB Academic Publishing, The Hague, Netherlands, pp. 63–76 (Chapter 6).
- Underwood, S.G., Steyer, G.D., Good, B., Chambers, D., 1991. Bay bottom terracing and vegetative planting: an innovative approach for habitat and water quality enhancement. In: Webb Jr., F.J. (Ed.), Annual Conference on Wetlands Restoration and Creation. Hillsborough Community College, Tampa, Florida, pp. 164–173.
- Ducks Unlimited, Inc., 2018. Geodatabase of Existing Marsh Terracing. Unpublished Material. Ducks Unlimited: Lafayette, La, USA.
- U.S. Army Corps of Engineers (USACE), 2014. Navigation conditions surveys. <https://www.mvn.usace.army.mil/Missions/Navigation/Channel-Surveys/>.
- U.S. Army Corps of Engineers (USACE), 2015. Use of Natural and Nature-Based Features (NNBF) for Coastal Resilience. Engineer Research and Development Center, Vicksburg, MS.
- U.S. Geological Survey, 2001. National Water Information System Data Available on the World Wide Web (Water Data for the Nation). <http://waterdata.usgs.gov/nwis/>.
- U.S. Geological Survey Coastal National Elevation Dataset, 2014. Topobathymetric Model of the Northern Gulf of Mexico, 1888 to 2013. <http://nationalmap.gov/viewer.html>.